Nano Research

ISSN 1998-0124 CN 11-5974/O4
https://doi.org/10.26599/NR.2026.94908915

Research Article

Robust and ultralow-energy direct photolithography of quantum dots via dual-ligand passivated thiol-ene click chemistry

Hao Tan[1,2,3], Zhixin Zhai[1,2], Chengjun Li[1,2,3], Kai Chen[1,2,3], Wenxuan Wang[1,2,3], Chang Gu[1,2](✉), Chaoyu Xiang[1,2], Ting Zhang[1,2](✉)

[1] Laboratory of Optoelectronic Information Technology and Devices, Ningbo Institute of Materials Technology and Engineering, Chinese Academy of Sciences, Ningbo 315201, China

[2] Hangzhou Bay Laboratory of Advanced Nano-Optoelectronic Materials and Devices, Qianwan Institute of CNITECH, Ningbo 315336, China

[3] School of Nano Science and Technology, University of Science and Technology of China, Suzhou 215123, China

Nano Res., **Just Accepted Manuscript** • https://doi.org/10.26599/NR.2026.94908915

https://www.sciopen.com/journal/1998-0124 on Jun. 6, 2026

Just Accepted

Nano Research

Open Access

Research Article

Robust and ultralow-energy direct photolithography of quantum dots via dual-ligand passivated thiol-ene click chemistry

Hao Tan[1,2,3], Zhixin Zhai[1,2], Chengjun Li[1,2,3], Kai Chen[1,2,3], Wenxuan Wang[1,2,3], Chang Gu[1,2,✉], Chaoyu Xiang[1,2], and Ting Zhang[1,2,✉]

[1] *Laboratory of Optoelectronic Information Technology and Devices, Ningbo Institute of Materials Technology and Engineering, Chinese Academy of Sciences, Ningbo 315201, China*
[2] *Hangzhou Bay Laboratory of Advanced Nano-Optoelectronic Materials and Devices, Qianwan Institute of CNITECH, Ningbo 315336, China*
[3] *School of Nano Science and Technology, University of Science and Technology of China, Suzhou 215123, China*

Received: 29 April 2026; **Revised:** 5 June 2026; **Accepted:** 6 June 2026

✉Address correspondence to Chang Gu, guchang@nimte.ac.cn; Ting Zhang, zhangting@nimte.ac.cn

Cite this article: *Nano Research*, 2026, 19, 94908915 https://doi.org/10.26599/NR.2026.94908915

ABSTRACT: Direct photolithography of colloidal quantum dots (QDs) via photoinitiated thiol-ene click chemistry has emerged as an attractive approach for the fabrication of high-resolution QD-based displays, benefiting from its site-controlled and byproduct-free reaction pathway. Nevertheless, this approach remains constrained by limited colloidal stability and suboptimal optoelectronic performance, stemming from spontaneous ligand exchange and unfavorable reaction kinetics. To address these challenges, we introduce a dual-ligand passivation strategy that replacing native QD ligands with rationally designed alkenyl ligands with strong binding affinity and high reactivity. This strategy confers a ~6-fold enhancement in the storage lifetime and a ~15-fold improvement in photolithographic efficiency. These advances enable the direct photopatterning of QDs with an ultrahigh resolution exceeding 18,000 PPI (pixel size: ~0.77 μm), at an ultralow-energy dose of ~1 mJ/cm². Furthermore, the fabricated light-emitting diode with the crosslinked DLP-QD and nano-patterned DLP-QD achieved peak external quantum efficiencies of 21.17% and 15.67%, respectively, ranking among the state-of-the-art devices in this field. This work demonstrates the promise of robust and efficient thiol-ene click chemistry enabled by dual-ligand passivation for direct QD photolithography, paving the way for high-performance QD-based displays and advanced optoelectronic devices toward industrial applications.

KEYWORDS: direct photolithography; dual-ligand passivation; thiol-ene click chemistry; high-resolution and nondestructive patterning; quantum dot light-emitting diodes

1 Introduction

Colloidal quantum dots (QDs) exhibit a range of advantageous properties, including tunable emission wavelengths, high photoluminescence quantum yields (PL QYs), narrow emission spectra, and solution processability, which collectively establish it as a promising candidate for next-generation high-quality displays [1-3]. To date, quantum dot light-emitting diodes (QLEDs) utilizing QDs as emissive layers have demonstrated exceptional performance. For example, external quantum efficiencies (EQEs) of red, green, and blue QLEDs have reached 44.5%, 29.2%, and 23%, respectively [4]. Furthermore, the fabrication of high-resolution non-destructive QD patterns has emerged as a crucial development direction [5], to meet the growing demand for enhanced visual experiences and the expanding application requirements in emerging display fields such as virtual reality (VR) and augmented reality (AR) interactions. To achieve this goal, several patterning approaches have been developed, including inkjet printing [6, 7], transfer printing [8, 9], and conventional photolithography [10, 11]. Nevertheless, significant challenges still remain, such as the coffee-ring effect [12], limited pattern fidelity for large-scale device applications [13], and photoresist residue and erosion to QDs [14], respectively.

Emerging direct photolithography of QDs enable efficient and high-throughput patterning by leveraging photochemical reactions of photosensitive ligands or additives to modulate the dispersibility of QDs [15-18]. Guided by this principle, several photolithographic schemes have been demonstrated, including in situ ligand exchange [19, 20], ligand cleavage [21, 22], and ligand crosslinking [23-25], achieving remarkable progress. However, most photolithography systems still exhibit limitations such as UV damage to QDs [26] and generation of byproducts (e.g., acids [27]), leading to performance degradation. Currently, there are still relatively few reports on photolithographic QLED devices achieving an EQE exceeding 20% [28-31], which still falls short when compared to that of state-of-the-art QLEDs without photolithographic processing [4, 32]. On this basis, developing efficient photolithography systems has been demonstrated to settle these challenges, and has become a

prominent research focus in the field.

Photoinitiated thiol-ene click chemistry has emerged as a transformative platform in precision manufacturing, featuring simple chemical structures and none byproducts [33-36]. Recently, this powerful strategy has been successfully extended to the direct photolithography of QDs, utilizing thiol-ene click chemistry reactions between thiol crosslinkers and native surface ligands of QDs or perovskite nanocrystals, such as oleylamine (OAm) and oleic acid (OA), opening new avenues for fabricating high-precision QD architectures [37-39]. However, the photochemical reaction efficiency in these systems is still suboptimal due to steric hindrance from the outer alkyl chains of OA/OAm ligands [40], leading a high-energy dose (>100 mJ/cm^2) [37, 39, 41] and potential UV damage of QDs. More critically, the strong binding affinity of thiol groups to QDs promotes spontaneous ligand exchange side reactions [42], leading to depletion of thiol crosslinkers and compromised stability of QDs, which poses significant challenges for long-term storage and large-scale industrial implementation. While reducing the polarity of thiol crosslinkers is expected to mitigate the stability issue [39], the concomitant low functionality considerably constrains the photolithographic efficiency. Therefore, the concurrent challenges of suboptimal reaction efficiency and insufficient stability represent critical bottlenecks that currently hinder the advancement of thiol-ene click chemistry in direct photolithography of QDs.

In this work, we proposed a dual-ligand passivation strategy to achieve robust and ultralow-energy thiol-ene click chemistry for direct QD photolithography through replacing the native ligands of QDs with rationally designed alkenyl ligands as functional ligands and alkyl thiols as dispersing ligands. The dual-ligand passivated QDs (designated as DLP-QD) effectively minimized undesirable ligand exchange side reactions and achieved an extended storage lifetime (>6-fold). Furthermore, the high reactivity of the designed alkenyl ligands enabled the DLP-QD system to produce well-defined photolithographic patterns at a substantially reduced energy dose (by one order of magnitude) without any damage in PL QYs. As a result, ultrahigh-resolution QD pixels (>18,000 PPI) were achieved at an ultralow-energy dose (~1 mJ/cm^2). And the fabricated QLEDs exhibited remarkable electroluminescent performance (for example, peak EQE > 21%), which represents state-of-the-art performance for photolithographic prototypes. Concurrently, QLEDs based on patterned DLP-QDs (< 1 μm) achieved an excellent performance (EQE > 15%), highlighting the potential of the dual-ligand passivation strategy for application in high-resolution, high-performance QLED devices. We anticipate that this strategy will release the considerable potential of direct photolithography of QDs via thiol-ene click chemistry for advancing high-resolution display technologies and facilitating large-scale industrial adoption, thereby accelerating the development of next-generation high-quality QD-based optoelectronic devices.

2 Result and Discussion

2.1 Dual-ligand passivation for stable thiol-ene click chemistry

Reported direct photolithography schemes of QDs via thiol-ene click chemistry commonly utilize photoinitiated crosslinking reactions between thiol crosslinkers and alkenyl groups (C=C) in the native ligands of QDs (e.g., OA, OAm), leading to the formation of crosslinked networks [37-39]. These systems frequently demonstrate harmful QDs aggregation and stability constraints [37]. As shown in **Fig. 1a**, the conventional thiol-ene photolithographic solution consisting of commonly used OA-capped red CdSe/ZnS core-shell QD (designated as OA-QD) and thiol crosslinker (pentaerythritol tetra(3-mercaptopropionate), PTMP) would generate substantial precipitation after 20 days of storage. This phenomenon could be further confirmed through dynamic light scattering (DLS) and UV-visible absorption spectra. As shown in **Fig. 1d**, the introduction of PTMP resulted in a rapid increase in particle size of OA-QD to approximately 20 nm. And the particle size reached the micrometer scale after 20 days, accompanied by a significant scattering signal (**Fig. 1e**). As a result, the spin-coated OA-QD/PTMP blended film displayed harmful QDs aggregation and inferior film quality even when prepared from fresh solutions (Fig. S1). Given the aggregation resulting from such a rapid spontaneous ligand exchange side reaction, it is not feasible to improve process operability simply by preparing fresh solutions immediately before use. Therefore, addressing the issue of colloidal stability at a fundamental level is highly necessary.

We propose that the observed phenomenon originates from the deprotonation of thiol groups in PTMP by OA on the QD surface. This reaction generates S^- species that coordinate to QDs [42], triggering spontaneous ligand exchange. Subsequently, the multiple thiol sites of PTMP anchor different QDs, leading to their aggregation and eventual precipitation. To validate this hypothesis, the chemical interaction between PTMP and OA-QD was analyzed. As shown in Fig. S2, ^{1}H NMR spectra of OA-QD/PTMP exhibited distinct characteristic signals of PTMP, indicating the successful binding of PTMP as a surface ligand. In addition, X-ray photoelectron spectroscopy (XPS) analysis revealed a notably decreased binding energy (0.31 eV) in the Zn 2p peaks of the OA-QD film with the addition of PTMP (**Fig. 1f**), further confirming the ligand exchange side reactions between PTMP and OA-QD [43].

To address the harmful ligand exchange and improve the system stability, we designed and proposed a dual-ligand passivation strategy, as shown in **Fig. 1b**. Here, the commonly used thiol ligand (1-dodecanethiol, 1-DT) was introduced as the dispersing ligand to replace the original OA ligand of OA-QD. And a rationally designed thiol-based ligand (dec-9-ene-1-thiol, DET) featuring a highly reactive terminal alkenyl group [44] was incorporated as the functional ligand to facilitate the photoinitiated thiol-ene click chemistry reaction. The synthesis details of DET were provided in Note S3 and Fig. S3. These ligands were introduced onto the QDs surface via solution-phase ligand exchange (Note S4), yielding dual-ligand passivated QDs (designated as DLP-QD). ^{1}H NMR results confirmed the

nearly complete replacement of pristine OA by 1-DT/DET (Fig. S4). The proportional distribution of the ligands was determined by calculating the integrated area ratios of characteristic peaks at distinct positions by the equations in Note S5. The calculation results were summarized in Table S1, which indicates that more than 85% of original OA ligands were successfully replaced by DET and 1-DT. Meanwhile, both photoluminescence (PL) spectra and UV-visible absorption spectra showed no significant changes before and after dual-ligand passivation (Fig. S5), indicating that this strategy did not affect the structural and optical characteristics of QDs. And the fluorescence lifetime of QDs increased after dual-ligand passivation, indicating effective passivation of surface defects (Fig. S5 and Table S2). In addition, the ligand contents on the QD surface before and after ligand exchange were characterized by thermogravimetric analysis (Fig. S6), and the ligand densities of the QDs were calculated. The calculation procedures and results were presented in Note S6 and Table S3, respectively. The results showed that the ligand density of DLP- QDs was approximately 3.64 nm^{-2}, which was slightly higher than that of OA- QDs (3.55 nm^{-2}), further confirming the effective passivation of surface defects.

To assess the effectiveness of the dual-ligand passivation strategy in improving system stability, the particle size distribution and UV-visible absorbance of the DLP-QD/PTMP system were systematically monitored. As shown in **Fig. 1d-e** and Fig. S7, the mixed solution retained nearly identical QD sizes and absorbance profiles even after 120-days storage, representing a 6-fold enhancement in storage lifetime compared to the original OA-QD/PTMP system. The as-prepared spin-coated film also exhibited markedly improved uniformity with significantly reduced QDs aggregation (Fig. S1). And XPS analysis confirmed minimal changes of binding energy in the Zn 2p peaks (**Fig. 1f**). These results validate the dual-ligand passivation strategy as an effective method to substantially enhance storage stability (**Fig. 1c**), thereby accelerating the industrialization of direct QDs photolithography via thiol-ene click chemistry.

Moreover, to further demonstrate the broad applicability of the stability enhancement, some other classical crosslinkers used in thiol-ene click chemistry were employed including pentaerythritol tetra(3-mercaptopropionate) (PTMA) [45] and 1,4-butanediol bis(thioglycolate) (BBT) [46]. As shown in Fig. S8 and S9, the OA-QD/PTMA system formed precipitates within 1 day, whereas the DLP-QD/PTMA system remained clear and stable for up to 30 days, representing an approximately 30-fold improvement in stability. Similarly, the DLP-QD/BBT system also exhibited significantly enhanced storage stability. These results confirm the broad potential of the dual-ligand passivation strategy, thus offering a generalizable foundation to advanced direct QDs photolithography via thiol-ene reactions.

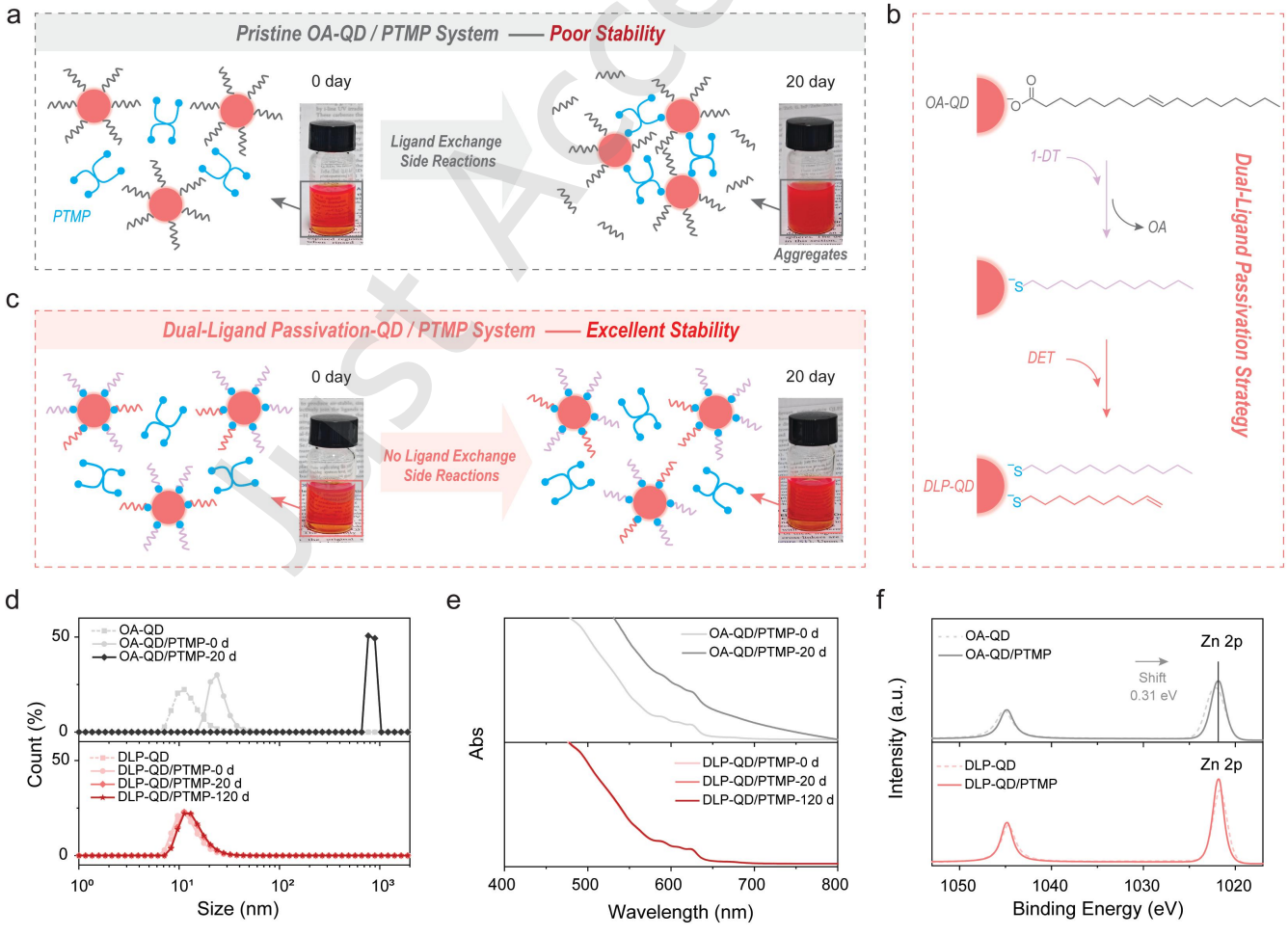

Figure 1 Stability enhancement of thiol-ene click chemistry via dual-ligand passivation strategy. (a) Schematic of the pristine OA-QD/PTMP system with poor stability due to spontaneous ligand exchange. The inset is the photo of the OA-QD/PTMP solution before and after 20-days storage. (b)

Schematic of dual-ligand passivation strategy with 1-DT and DET. (c) Schematic of the DLP-QD/PTMP system with excellent stability. The inset is the photo of the DLP-QD/PTMP solution before and after 20-days storage. (s) Size distribution of OA-QD (top) and DLP-QD (bottom) with and without PTMP in toluene for different days. (e) UV-vis absorption spectra of OA-QD (top) and DLP-QD (bottom) with PTMP in toluene for different days. (f) XPS spectra of OA-QD (top) and DLP-QD (bottom) films with and without PTMP.

2.2 High-efficient photolithography of DLP-QD via thiol-ene click chemistry

In reported thiol-ene-based direct photolithography system of QDs, although the conventional OA ligands contain alkenyl sites, the steric hindrance imposed by its long outer alkyl chain tends to restrict its reactivity [40]. To address this limitation, the dual-ligand passivation strategy we developed incorporates the functional ligand (DET) with a highly reactive terminal alkenyl group (Fig. S10). As shown in **Fig. 2a**, under UV irradiation, thiyl radicals are generated by the photolysis of the S-H bonds from PTMP and react with the highly reactive C=C bonds of DET, leading to the crosslinking of QDs through the covalent bonding, which effectively reduces the solubility of QDs. As a proof of concept, a series of DLP-QD films with different photolithographic parameters were fabricated on silicon substrates, and QD pixel arrays were generated by using a patterned photomask. The patterning procedure is detailed in the Note S7 and Fig. S11.

As shown in Fig. S12, the fluorescence intensity of QD patterns progressively enhanced with the increasing PTMP content, with the optimal patterning resolution achieved at a PTMP content of 10 wt%. With the PTMP content fixed at 10 wt%, the effect of exposure dose on the patterning resolution was investigated. Results revealed that a low-energy dose of 10 mJ/cm^2 under 254 nm UV exposure was sufficient to produce well-defined QD patterns (**Fig. 2b**), which was significantly lower than the typical doses (> 100 mJ/cm^2) required in conventional thiol-ene direct photolithography systems based on OA/OAm ligands [37, 39, 41]. Here, a 254 nm source was selected for photolithographic exposure instead of the commercially prevalent i- line (365 nm), based on the fact that PTMP exhibits substantially higher photosensitivity at 254 nm (Fig. S13). As a contrast, a minimum dose exceeding 200 mJ/cm^2 was required to achieve well-defined QD patterns under i-line exposure (Fig. S14).

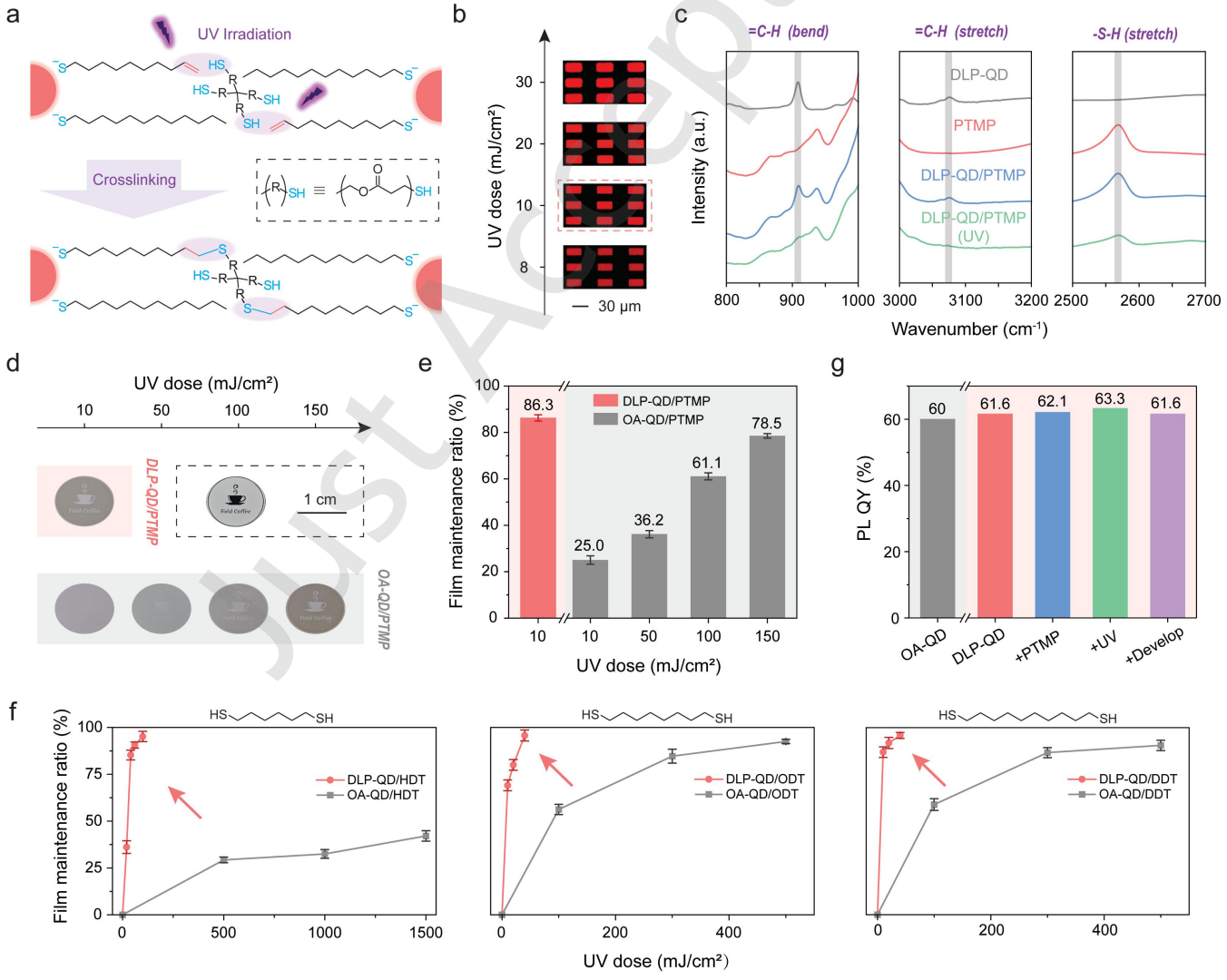

Figure 2 Direct photolithography of DLP-QD via thiol-ene click chemistry. (a) Schematic of photolithographic mechanism of DLP-QD. (b) Fluorescence microscopic images of photolithographic DLP-QD patterns with various UV doses. (c) FT-IR spectra of DLP-QD, PTMP, and DLP-QD/PTMP before and after UV exposure. (d) Photos of photolithographic OA-QD and DLP-QD patterns with PTMP under various UV doses. Insert: photo of the photomask. (e) Film maintenance ratio of patterned OA-QD and DLP-QD with various UV doses. (f) Film maintenance ratio of photolithographic OA-QD and DLP-QD

using HDT, ODT and DDT with various UV doses. (g) PL QYs of OA-QD film and DLP-QD films at different photolithographic stages.

Fourier transform infrared (FT-IR) spectroscopy was employed to monitor the thiol-ene reaction process. As shown in **Fig. 2c**, the FTIR spectrum of the DLP-QD/PTMP exhibited characteristic signals from both PTMP (e.g., the S-H stretching vibration at 2568 cm^{-1}) and the surface ligands of DLP-QD (e.g., the bending and stretching vibrations of =C-H bonds at 909 cm^{-1} and 3075 cm^{-1}) [47]. After UV exposure, the disappearance of the =C-H-related signal and the decreased intensity of the S-H signal confirmed the occurrence of the expected thiol-ene reaction. In contrast, DLP-QD without PTMP failed to produce photolithographic patterns (Fig. S15), validating the necessity of PTMP and further supporting the proposed crosslinking mechanism.

A comprehensive comparison was further conducted to validate the effectiveness of dual-ligand passivation in enhancing the photolithographic reactivity. As shown in **Fig. 2d**, an exposure dose of >150 mJ/cm^2 was required to achieve photolithographic patterns in the original OA-QD/PTMP system. In contrast, comparable patterning quality could be achieved at a significantly lower dose of only ~10 mJ/cm^2 in the DLP-QD/PTMP system. This phenomenon was further verified by the film maintenance ratio after patterning, as shown in **Fig. 2e**. The definition and calculation details of film maintenance ratio were provided in Note S8. That is to say, the reaction efficiency of direct photolithography system of QDs was markedly improved by the dual-ligand passivation strategy as we designed, which reduced the required exposure dose by at least an order of magnitude. Notably, the ligand densities of DET and residual OA in the DLP- QDs were 1.35 nm^{-2} and 0.51 nm^{-2} (Table S3), respectively, significantly lower than the OA ligand density of OA- QDs (3.55 nm^{-2}), indicating that the content of C=C bonds in DLP- QDs was lower than that in OA- QDs. Nevertheless, DLP- QDs exhibited a significantly reduced exposure dose (**Fig. 2d-e**). These findings indicated that the high photolithographic reaction efficiency of the DLP- QD system originated from the high reactivity of the DET ligands.

To demonstrate the general applicability of the dual-ligand passivation strategy in improving the photolithographic efficiency, an extended validation was performed using aliphatic thiol crosslinkers with lower polarity and fewer reactive sites, such as 1,6-hexanedithiol (HDT), 1,8-octanedithiol (ODT), and 1,10-decanedithiol (DDT). As shown in **Fig. 2f**, the DLP-QD/HDT system reached a high film maintenance ratio exceeding 90% at an exposure dose of 60 mJ/cm^2. In contrast, the OA-QD/HDT system showed poor photo-crosslinking results even at a high dose of 1500 mJ/cm^2, with a low film maintenance ratio below 50%. Although a moderate improvement for OA-QD could be achieved through increasing chain length of crosslinkers, attributed to enhanced crosslinking probability between adjacent QDs [39], the photolithographic outcomes remained substantially inferior to that of DLP-QD (**Fig. 2f**). These results further demonstrate that the dual-ligand passivation expands the materials candidates of thiol crosslinkers for thiol-ene-based QD photolithography, establishing a robust foundation for the application of direct photolithography of QDs in emerging display technologies.

Benefiting from the efficiency and stability improvement of the developed thiol-ene click chemistry system based on dual-ligand passivation, nondestructive QDs photolithography was successfully achieved. PL QY measurements revealed that DLP-QD exhibited an improvement of approximately 3% compared to OA-QD (**Fig. 2g**), which could be attributed to the defect- passivation effect conferred by the thiol ligands [25, 48]. Notably, the PL QYs of DLP-QD further increased after the incorporation of PTMP and UV irradiation. This enhancement was ascribed to the increased distance between adjacent QDs resulting from the photochemical crosslinking process, which reduces fluorescence quenching between adjacent QDs [37]. This interpretation was supported by grazing-incidence small-angle X-ray scattering (GISAXS) results, which indicated that the average distance between adjacent QDs increased from 13.61 nm to 13.98 nm following PTMP incorporation and UV irradiation (Fig. S13 and Note S9). Although a slight reduction in PL QY was observed after development, which could be attributed to the removal of loosely bound surface species and a slight degradation in QD film quality (Fig. S17) [25], the value remained higher than that of pristine OA-QD, yielding a final PL QY retention of ~103%. Compared to the pristine OA-QD film that exhibited a surface roughness (arithmetic average height, Ra) of 1.91 nm, the DLP-QD film demonstrated a lower Ra value (1.59 nm), demonstrating good film quality. Although the Ra value of the DLP-QD film increased to 1.81 nm upon blending with PTMP, the final roughness of the DLP-QD/PTMP film after UV exposure and developing remained lower than that of the pristine OA-QD film.

2.3 High-resolution patterns based on direct photolithographic DLP-QDs

High-precision patterning was achieved with photolithographic DLP-QD based on dual-ligand passivation strategy, as exemplified by closely packed circular pixel arrays (pixel size = ~5 μm), as shown in **Fig. 3a**. This capability made the system highly suitable for high-resolution displays, such as near-eye displays. Pixel arrays under varying resolutions and periodic arrangements were further demonstrated in **Fig. 3b-c** and Fig. S18, with an ultrahigh resolution reaching approximately >18,000 PPI (pixel size ≈ 0.77 μm). Meanwhile, the patterning resolution potential of the OA-QD/PTMP system was investigated. As shown in Fig. S19, the results indicated that although high-resolution features could be partially achieved, significant background residue remained in the non-pixelated areas. The unexposed regions could not be completely removed during development, which was attributed to QD aggregation caused by spontaneous ligand exchange side reactions. Furthermore, under identical PTMP content, the OA-QD/PTMP system required a substantially higher exposure dose (100 mJ/cm^2) to achieve patterning, whereas the DLP-QD/PTMP system only required an exposure dose of 10 mJ/cm^2. These results further substantiated the superior efficacy of the dual-ligand passivation strategy. As an extension of this strategy, it had been successfully applied to green and blue QDs (Fig. S20 and Fig. S21), leading to the fabrication of corresponding ultrahigh-resolution

photolithographic patterns (**Fig. 3a-c**). Remarkably, the green QDs system based on the dual-ligand passivation strategy only required an extremely low exposure dose of ~1 mJ/cm^2 during the photolithographic process, which was obtained under optimized exposure dose conditions (Fig. S22). To the best of our knowledge, this level of resolution and exposure dose represents a state-of-the-art performance compared with other reported direct QDs photolithography systems (**Fig. 3d** and Table S4). Such ultrahigh-resolution QD arrays, which far exceeding the resolving power of the human eye, might provide an essential hardware foundation for developing scalable quantum chips.

The superior patterning capability of DLP-QD in generating diverse and intricate patterns required for practical applications was demonstrated in **Fig. 3e**, while the QD patterns maintained excellent color fidelity with well-preserved PL spectra after photolithography. Moreover, the photolithographic DLP-QDs exhibited remarkable substrate compatibility, successfully extending to silicon, transparent glass, and flexible polyethylene terephthalate (PET) substrates (**Fig. 3f**), as validated using a flower-patterned photomask. Furthermore, the dual-ligand passivation strategy was proved effective for the photolithographic patterning of InP-based QDs (**Fig. 3g**), highlighting its broad material applicability.

The photolithographic DLP-QD films exhibited exceptional solvent resistance, thus enabling the fabrication of multicolor QD patterns through lateral overlay (**Fig. 3h**) or vertical stacking of different QD layers (Fig. S23). And the overlaid patterns exhibited no color crosstalk and demonstrated excellent contrast, substantiating the potential of the proposed strategy for practical display applications.

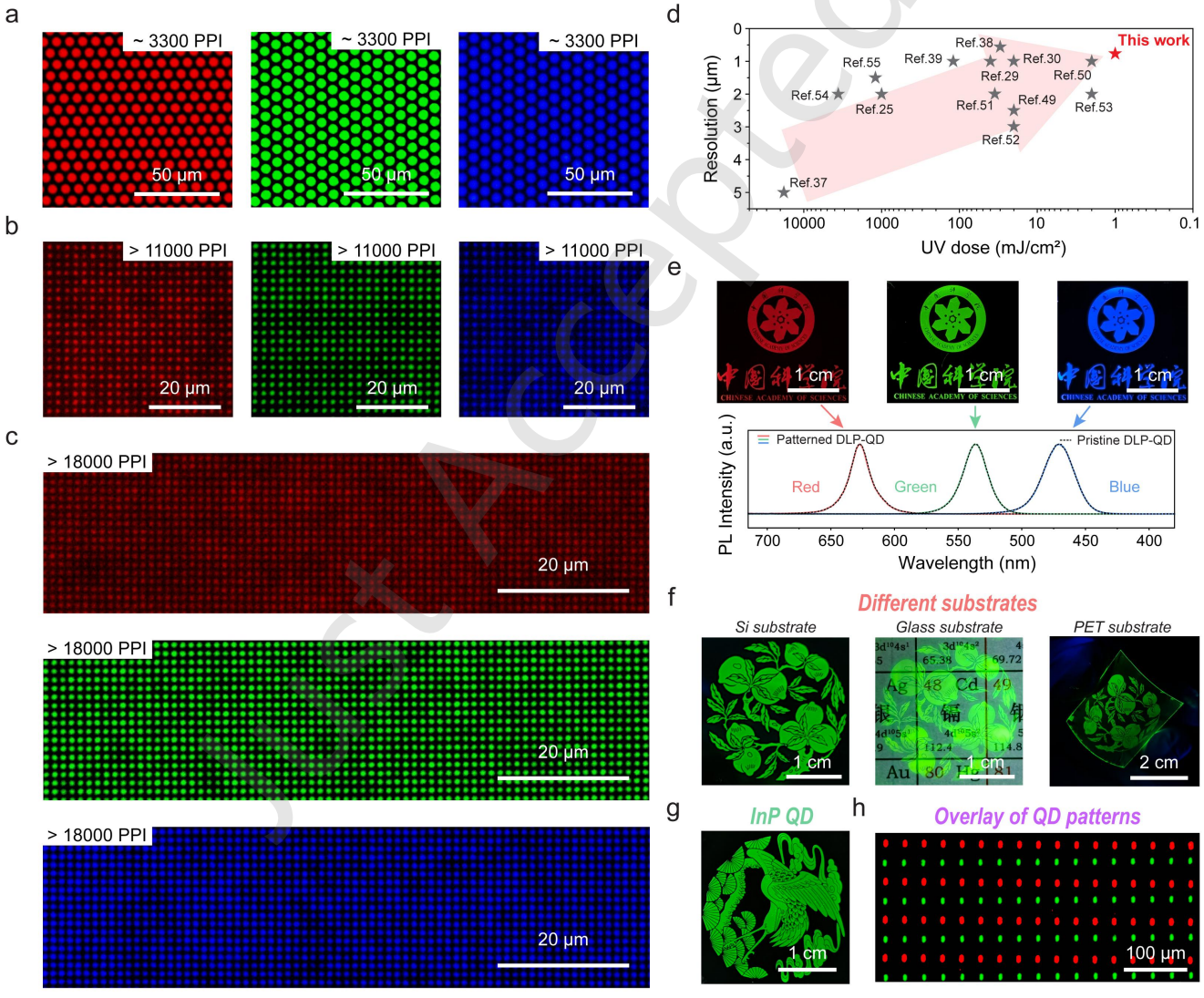

Figure 3 Direct photolithographic multi-color patterns of DLP-QD. (a-c) Fluorescence microscopic images of pixel arrays of RGB DLP-QDs prepared by different photomasks. (d) Comparison of pattern resolution and UV dose of photolithographic QDs based on different photosensitive crosslinkers [25, 29, 30, 37-39, 49-55]. (e) Fluorescence images (top) and PL spectra (bottom) of photolithographic multi-color QD patterns. (f) Fluorescence images of photolithographic DLP-QD patterns on different substrates. (g-h) Fluorescence images of InP-based QD pattern (g) and overlay of QD patterns (h).

2.4 Efficient QLEDs based on direct photolithographic DLP-QDs

To evaluate the potential of the as-developed dual-ligand passivated thiol-ene click chemistry for optoelectronic displays, the optoelectronic characteristics of QLEDs employing either pristine QD or photolithographic DLP-QD as the emission layers were measured (**Fig. 4a** and Note S10). To enable a rigorous and unambiguous comparison of device performance with and without QD crosslinking, the

emissive layer was deliberately left non-patterned. This ensures identical emission area and device geometry across all comparative devices, offering greater credibility in evaluating the effect of crosslinking on device performance. The QLEDs incorporated poly(3,4-ethylenedioxythiophene): poly(styrenesulfonate) (PEDOT: PSS) and ZnO nanoparticles as the hole injection layer (HIL) and the electron transport layer (ETL), respectively. And a thermal-cured poly(9,9-dioctylfluorenyl-2,7-diyl)-co-(4,4'-(N-(p-butylphenyl))diphenylamine) (X1-TFB) was applied as the hole transport layer (HTL) to avoid the potential interlayer erosion [18]. The energy band diagram depicted in **Fig. 4b** was constructed using valence and conduction band levels determined by references and ultraviolet photoelectron spectroscopy (UPS).

Benefitting from the upshifted energy levels of the QD layers, induced by dual-ligand passivation and the photolithographic process, the hole injection barrier was reduced while the electron injection barrier was raised, leading to more balanced charge carrier injection within the device. Furthermore, corresponding hole-only devices (HODs) with the structure of ITO/PEDOTPSS/X1-TFB/QDs/Au and electron-only devices (EODs) with the structure of ITO/ZnO/QDs/ZnO/Ag were fabricated to systematically investigate carrier mobility characteristics. As shown in Fig. S24, the current density of HOD based on photolithographic DLP-QD exhibited higher current density than that of HOD based on pristine QD, whereas the current density in related EOD was significantly lower. This phenomenon was attributed to the rise in energy level resulting from crosslinking and ligand exchange, which facilitated more balanced charge injection and transport within the device. And the QLED based on photolithographic DLP-QD achieved a peak EQE of 21.17% (**Fig. 4c**), representing a leading performance in the field of direct photolithography of QDs (Table S4) and exceeding the peak EQE of the reference QLED based on pristine QD (19.57%). The statistical distribution of the peak EQEs was

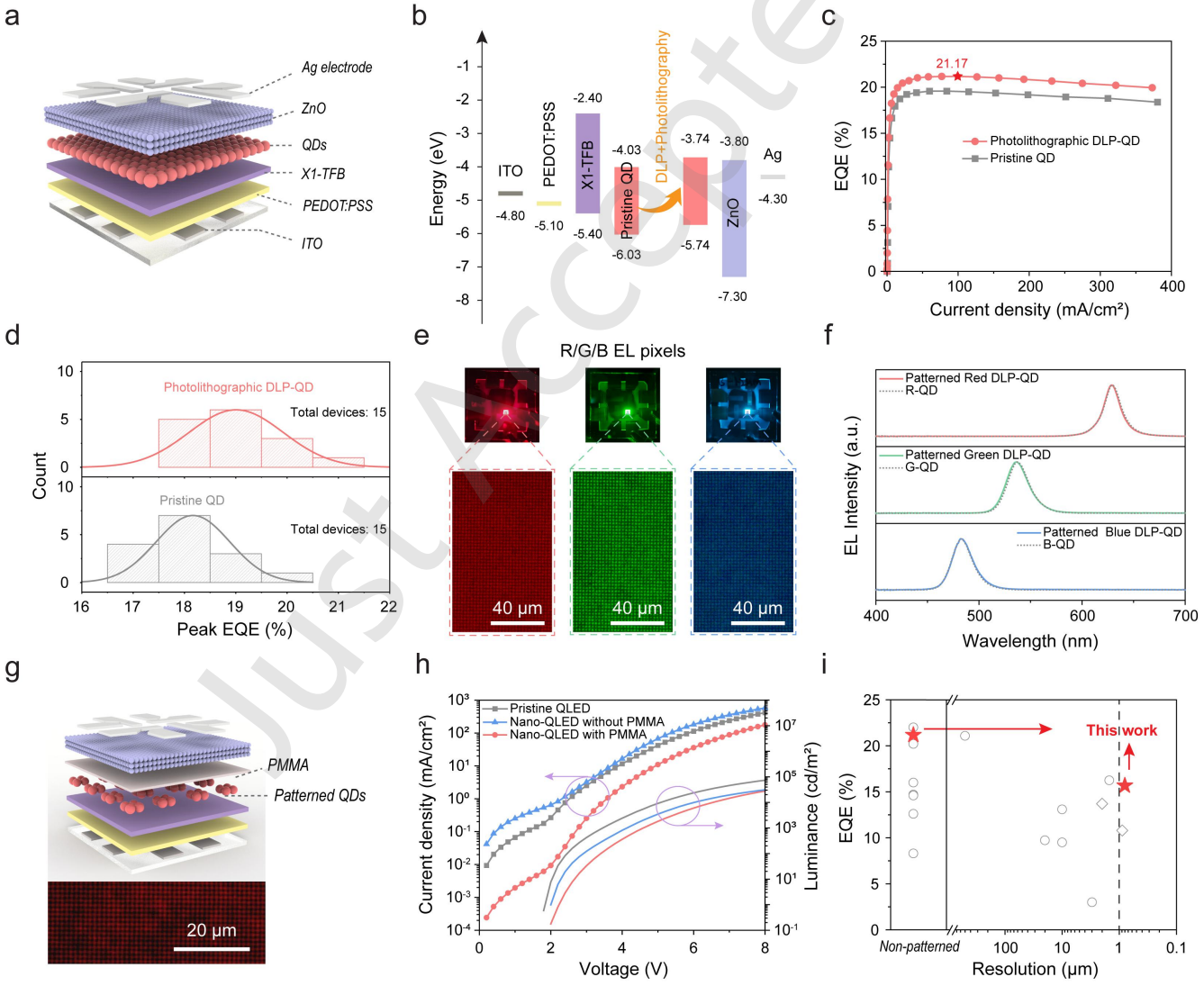

Figure 4 High-performance QLEDs based on direct photolithographic DLP-QD. (a-b) Schematic of QLED device structure (a) and related energy band diagram (b). (c) Current density dependent EQEs of QLEDs implementing pristine QD and photolithographic DLP-QD. (d) Statistical distribution of peak EQE of QLEDs. (e) Microscopic EL images of patterned QLEDs implementing photolithographic RGB DLP-QDs. (f) EL intensity QLEDs based on pristine Red/Green/Blue QDs and patterned Red/Green/Blue DLP-QDs. (g) Schematic of patterned QLED device structure. Insert: microscopic EL image of Nano-QLED. (h) Current density-voltage-luminance characteristics of pristine QLED, Nano-QLED without PMMA, and Nano-QLED with PMMA. (i) Comparison of peak EQE (including non-patterned and patterned QLED) and EL pixel resolution for EL devices fabricated via photolithography (Circles represent direct photolithography schemes. Diamonds represent conventional photolithography schemes.) [5, 25, 28-30, 38, 39, 49-56].

evaluated across 15 devices for each type. As shown in **Fig. 4d**, the QLEDs based on photolithographic DLP-QD exhibited an average peak EQE of 19.01% ± 0.92%, outperforming that of the devices based on pristine QD (18.17% ± 0.72%), which confirmed the beneficial effect of dual-ligand passivation strategy. On the other hand, a general reduction in current density was observed in the photolithographic QLED devices (Fig. S25), which could be attributed to the increased distance between adjacent QDs after crosslinking, thereby reducing charge transport efficiency [37], and this finding was consistent with the previous GISAXS results (Fig. S16).

Furthermore, as shown in **Fig. 4e** and **4f**, high-resolution RGB electroluminescent (EL) pixels with a feature size of 1.2 μm (> 11,000 PPI) were successfully demonstrated, while the peak positions and full width at half maximum of the electroluminescence spectra remained virtually unchanged after the photolithography process, confirming the excellent color fidelity. However, in QLED devices with patterned QD films, the direct contact between the ETL and the HTL within non-patterned regions induces significant leakage current, thereby degrading device performance [17]. To solve this problem, an additional electron-blocking layer composed of PMMA was introduced between the patterned QD layer and the ZnO layer to suppress leakage current in non-patterned areas. A schematic of the patterned device was presented in **Fig. 4g**. Subsequently, QLEDs were fabricated using both pristine QD and patterned DLP-QD as the emissive layers, with the aforementioned PMMA interlayer incorporated in both device architectures. The QLED based on patterned DLP-QD (with a minimum feature size of ~0.80 μm, designated as Nano-QLED) achieved a peak EQE of 15.67% (Fig. S26), comparable to non-patterned pristine QLED without significant leakage current (**Fig. 4h**). These achievements represent an attractive value for EL devices fabricated via photolithography (**Fig. 4i** and Table S4), highlighting the potential of direct QD photolithography system based on dual-ligand passivation for future high-resolution multi-color display applications. However, we also note that the overall performance of pixelated QLED devices fabricated by photolithography still lags behind that of those fabricated by state-of-the-art transfer printing approaches [57, 58], which represents a critical challenge that urgently needs to be addressed in the field of photolithography.

3 Conclusions

In summary, this work presented a novel dual-ligand passivation strategy for addressing the stability and photolithographic efficiency limitations of direct QD photolithography based on thiol-ene click chemistry. Comprehensive characterization through DLS, UV-visible spectra, and XPS analysis confirmed a more than 6-fold enhancement in storage stability due to suppressed spontaneous ligand exchange. Furthermore, by incorporating a rationally designed terminal-alkenyl ligand with high photochemical reactivity, the required exposure dose of photolithographic patterning was reduced by at least an order of magnitude. This advancement enabled the successful fabrication of ultrahigh-resolution QD pixel arrays (> 18,000 PPI) under an ultralow-energy dose of ~1 mJ/cm^2. And the strategy enhanced the PL QY of QDs following photolithography without any post-treatment. Additionally, QLED devices based on photolithographic DLP-QD and patterned DLP-QD exhibited notably high electroluminescent performance (e.g., a peak EQE of 21.17% for non-patterned QLED and a peak EQE of 15.67% for Nano-QLED), representing state-of-the-art values in the field. The successful implementation of the dual-ligand passivation strategy paves the way for improving the storage stability and optical processing efficiency of direct thiol-ene photolithography of QDs, highlighting its substantial potential to facilitate the development of next-generation high-resolution and high-performance optoelectronic devices.

Acknowledgements

This study was supported by the National Natural Science Foundation of China (No. 62404227), the Zhejiang Provincial Natural Science Foundation of China (No. LMS26E020007), Ningbo young doctor innovative research project (No. 2025J030), the Key projects of National Natural Science Foundation of China (No. 62234004), "Pioneer" and "Leading Goose" R&D Program of Zhejiang (Nos. 2024C01191), the Hangzhou Joint Fund of Zhejiang Provincial Natural Science Foundation of China under Grant (No.HZSZ26E020005), Ningbo 3315 Programme (No. 2020A-01-B), YONGJIANG Talent Introduction Programme (Nos. 2021A-038-B), and Ningbo Science and Technology Yongjiang 2035 Key Technology Breakthrough Plan Project (Nos. 2025Z079, 2024Z146). The authors thank Ben He for his suggestions on molecular synthesis and the preliminary design of this work.

Author contribution statement

H. T.: Data curation, Investigation, Writing - original draft, Writing - review & editing. Z. X. Z.: Formal analysis, Investigation. C. J. L.: Formal analysis, Investigation. K. C.: Formal analysis, Investigation. W. X. W.: Formal analysis, Investigation. C. G.: Investigation, Writing - review & editing, Writing - original draft, Funding acquisition. C. Y. X.: Funding acquisition. T. Z.: Conceptualization, Funding acquisition, Writing - review & editing. All authors discussed the results and commented on the manuscript.

Declaration of competing interest

All the contributing authors report no conflict of interests in this
work.

References

[1] García de Arquer, F. P.; Talapin, D. V.; Klimov, V. I.; Arakawa, Y.; Bayer, M.; Sargent, E. H. Semiconductor quantum dots: Technological progress and future challenges. *Science* **2021**, *373*, eaaz8541.

[2] Fan, J.; Han, C.; Yang, G.; Song, B.; Xu, R.; Xiang, C.; Zhang, T.; and Qian, L. Recent Progress of Quantum Dots Light-Emitting Diodes: Materials, Device Structures, and Display Applications. *Adv. Mater.* **2024**, *36*, 2312948.

[3] Jang, E.; Jang, H. Review: Quantum Dot Light-Emitting Diodes. *Chem. Rev.* **2023**, *123*, 4663-4692.

[4] Shen, Z.; Zhang, F.; Shen, H.; and Li, H. Green Emissive Electroluminescent Devices Based on Colloidal Quantum Dots. *Adv. Funct. Mater.* **2025**, *35*, 2422093.

[5] Lian, Y.; Wang, Y.; Yuan, Y.; Ren, Z.; Tang, W.; Liu, Z.; Xing, S.; Ji, K.; Yuan, B.; Yang, Y. et al. Downscaling micro- and nano-perovskite LEDs. *Nature* **2025**, *640*, 62-68.

[6] Xiang, C.; Wu, L.; Lu, Z.; Li, M.; Wen, Y.; Yang, Y.; Liu, W.; Zhang, T.; Cao, W.; Tsang, S. et al. High efficiency and stability of ink-jet printed quantum dot light emitting diodes. *Nat. Commun.* **2020**, *11*, 1646.

[7] Shi, L.; Meng, L.; Jiang, F.; Ge, Y.; Li, F.; Wu, X.; Zhong, H. In Situ Inkjet Printing Strategy for Fabricating Perovskite Quantum Dot Patterns. *Adv. Funct. Mater.* **2019**, *29*, 1903648.

[8] Meng, T.; Zheng, Y.; Zhao, D.; Hu, H.; Zhu, Y.; Xu, Z.; Ju, S.; Jing, J.; Chen, X.; Gao, H. et al. Ultrahigh-resolution quantum-dot light-emitting diodes. *Nat. Photonics* **2022**, *16*, 297-303.

[9] Yoo, J.; Lee, K.; Yang, U. J.; Song, H. H.; Jang, J. H.; Lee, G. H.; Bootharaju, M. S.; Kim, J. H.; Kim, K.; Park, S. I. et al. Highly efficient printed quantum dot light-emitting diodes through ultrahigh-definition double-layer transfer printing. *Nat. Photonics* **2024**, *18*, 1105-1112.

[10] Park, J. S.; Kyhm, J.; Kim, H. H.; Jeong, S.; Kang, J.; Lee, S. E.; Lee, K. T.; Park, K.; Barange, N.; Han, J. et al. Alternative Patterning Process for Realization of Large-Area, Full-Color, Active Quantum Dot Display. *Nano Lett.* **2016**, *16*, 6946-6953.

[11] Park, S. Y.; Lee, S.; Yang, J.; Kang, M. S. Patterning Quantum Dots via Photolithography: A Review. *Adv. Mater.* **2023**, *35*, 2300546.

[12] Jiang, C.; Zhong, Z.; Liu, B.; He, Z.; Zou, J.; Wang, L.; Wang, J.; Peng, J.; Cao, Y. Coffee-Ring-Free Quantum Dot Thin Film Using Inkjet Printing from a Mixed-Solvent System on Modified ZnO Transport Layer for Light-Emitting Devices. *ACS Appl. Mater. Interfaces* **2016**, *8*, 26162-26168.

[13] Lee, J.; Jo, H.; Choi, M.; Park, S.; Oh, J.; Lee, K.; Bae, Y.; Rhee, S.; Roh, J. Recent Progress on Quantum Dot Patterning Technologies for Commercialization of QD-LEDs: Current Status, Future Prospects, and Exploratory Approaches. *Small Methods* **2024**, *8*, 2301224.

[14] Qiu, Y.; Yu, Y.; Wang, S.; Chen, M. Advances in Quantum Dot Direct Photolithographic Patterning. *ACS Mater. Lett.* **2024**, *6*, 3176-3189.

[15] Hahm, D.; Lim, J.; Kim, H.; Shin, J. W.; Hwang, S.; Rhee, S.; Chang, J. H.; Yang, J.; Lim, C. H.; Jo, H. et al. Direct patterning of colloidal quantum dots with adaptable dual-ligand surface. *Nat. Nanotechnol.* **2022**, *17*, 952-958.

[16] Fan, J.; Qian, L. Quantum dot patterning by direct photolithography. *Nat. Nanotechnol.* **2022**, *17*, 906-907.

[17] Gu, C.; Zhai, Z.; Wang, W.; Tan, H.; Ding, S.; Fan, J.; Qian, L.; Zhang, T.; Xiang, C. Ultra-high-resolution nondestructive photolithography of quantum dots enabled by photo-shield crosslinker. *Mater. Today* **2025**, *89*, 100-106.

[18] Zhai, Z.; Gu, C.; Wang, W.; Tan, H.; Han, C.; Zhang, T.; Xiang, C. Nondestructive direct photolithography of colloidal quantum dots enabled by benzophenone-based crosslinkers. *Nano Res.* **2025**, *18*, 94907980.

[19] Wang, Y.; Fedin, I.; Zhang, H.; Talapin, D. V. Direct optical lithography of functional inorganic nanomaterials. *Science* **2017**, *357*, 385-388.

[20] Lee, J.; Ha, J.; Lee, H.; Cho, H.; Lee, D. C.; Talapin, D. V.; Cho, H. Direct Optical Lithography of Colloidal InP-Based Quantum Dots with Ligand Pair Treatment. *ACS Energy Lett.* **2023**, *8*, 4210-4217.

[21] Pan, J. A.; Ondry, J. C.; Talapin, D. V. Direct Optical Lithography of $CsPbX_3$ Nanocrystals via Photoinduced Ligand Cleavage with Postpatterning Chemical Modification and Electronic Coupling. *Nano Lett.* **2021**, *21*, 7609-7616.

[22] Lee, J.; Yeon, S.; Koo, B.; Sohn, B.; Park, S. J.; Kim, C.; Cho, H. Photocleavable Ligand-Induced Direct Photolithography of InP-Based Quantum Dots. *ACS Energy Lett.* **2025**, *10*, 94-101.

[23] Xiao, P.; Ma, J.; Zhang, Z.; Zou, Y.; Luo, H.; Guan, J.; Zhang, J.; Zhou, L.; Hou, W.; Zhang, P. et al. Ligand-Engineered Direct Optical Lithography of Nanocrystals with Industrially Compatible Solvents. *ACS Nano* **2025**, *19*, 14509-14520.

[24] Liu, D.; Weng, K.; Lu, S.; Li, F.; Abudukeremu, H.; Zhang, L.; Yang, Y.; Hou, J.; Qiu, H.; Fu, Z. et al. Direct optical patterning of perovskite nanocrystals with ligand cross-linkers. *Sci. Adv.* **2022**, *8*, eabm8433.

[25] Lee, N.; Choi, D.; Ko, K. J.; Kim, H. S.; Yu, J. H.; Lee, J. S. Direct Optical Lithography Using Diazirine Cross-Linker for Quantum Dot Light Emitting Diodes and Enhancing Photoluminescence Quantum Yield through Post-treatment. *ACS Nano* **2025**, *19*, 22253-22261.

[26] Qing, W.; Si, Y.; Cai, M.; Zhou, L.; Wu, L.; Hou, Z.; Liu, D.; Tian, X.; Liu, W.; Lin, L. et al. Photosensitizer-assisted direct 2D patterning and 3D printing of colloidal quantum dots. *Nano Res.* **2024**, *17*, 10460-10466.

[27] Cho, H.; Pan, J. A.; Wu, H.; Lan, X.; Coropceanu, I.; Wang, Y.; Cho, W.; Hill, E. A.; Anderson, J. S.; Talapin, D. V. Direct Optical Patterning of Quantum Dot Light-Emitting Diodes via In Situ Ligand Exchange. *Adv. Mater.* **2020**, *32*, 2003805.

[28] Xiao, P.; Ma, J.; Zhang, Z.; Zou, Y.; Luo, H.; Guan, J.; Zhang, J.; Zhou et al. Ligand-engineered direct optical lithography of nanocrystals with industrially compatible solvents. *ACS Nano* **2025**, *19*, 14509-14520.

[29] Chen, Z.; Man, Z.; Rao, S.; Zhao, J.; Wang, S.; Zhang, R.; Teng, F.; Tang, A. Rigid crosslinker-assisted nondestructive direct photolithograph for patterned QLED displays. *Light Sci. Appl.* **2025**, *14*, 251.

[30] Guan, J.; Ma, J.; Zhou, L.; Zou, Y.; Ye, L.; Hou, W.; Zhang, P.; Dai, X.; Zhang, H.; Talapin, D. V. et al. Direct ambient photopatterning of RGB quantum dots for light-emitting diodes with EQE exceeding 20%. *Nat. Commun.* **2025**, *16*, 9689.

[31] Zhang, H.; Fu, Z.; Qing, W.; Liu, W.; Tian, X.; Li, J. Surface Photochemistry Enabled Direct Patterning of Colloidal Inorganic Nanocrystals: From 2D to 3D. *Chem. Rev.* **2026**, *126*, 3624-3663.

[32] Zhang, W.; Li, B.; Chang, C.; Chen, F.; Zhang, Q.; Lin, Q.; Wang, L.; Yan, J.; Wang, F.; Chong, Y. et al. Stable and efficient pure blue quantum-dot LEDs enabled by inserting an anti-oxidation layer. *Nat. Commun.* **2024**, *15*, 783.

[33] Hoyle, C. E.; and Bowman, C. N. Thiol–Ene Click Chemistry. *Angew. Chem., Int. Edit.* **2010**, *49*, 1540-1573.

[34] Zhong, D.; Wu, C.; Jiang, Y.; Yuan, Y.; Kim, M. G.; Nishio, Y.; Shih, C. C.; Wang, W.; Lai, J. C.; Ji, X. et al. High-speed and large-scale intrinsically stretchable integrated circuits. *Nature* **2024**, *627*, 313-320.

[35] Tang, Z. B.; Bian, L.; Miao, X.; Gao, H.; Liu, L.; Jiang, Q.; Shen, D.; Xu, L.; Sue, A. C. H.; Zheng, X. et al. Synthesis of a crystalline two-dimensional [c2]daisy chain honeycomb network. *Nat. Synth.* **2025**, *4*, 922-930.

[36] Wang, Q.; Cui, H.; Wang, X.; Hu, Z.; Tao, P.; Li, M.; Wang, J.; Tang, Y.; Xu, H.; He, X. Exceptional Light Sensitivity by Thiol-Ene Click Lithography. *J. Am. Chem. Soc.* **2023**, *145*, 3064-3074.

[37] Shin, S.; Kang, K.; Jang, H.; Gwak, N.; Kim, S.; Kim, T. A.; Oh, N. Ligand-Crosslinking Strategy for Efficient Quantum Dot Light-Emitting Diodes via Thiol-Ene Click Chemistry. *Small Methods* **2023**, *7*, 2300206.

[38] Maeng, S.; Park, S. J.; Lee, J.; Lee, H.; Choi, J.; Kang, J. K.; Cho, H. Direct photocatalytic patterning of colloidal emissive nanomaterials. *Sci. Adv.* **2023**, *9*, eadi6950.

[39] Maeng, S.; Kim, J.; Kim, T.; Lee, S.; Han, S.; Park, S. J.; Kim, C.; Kim, J.; Lee, J. Y.; Cho, H. Dual-Strategy Direct Photocatalytic Patterning for Efficient Perovskite Nanocrystal LED Displays. *Adv. Mater.* **2025**, *37*, e08217.

[40] Yeon, S.; Kim, Y.; Adel, A. E.; Ha, J.; Maeng, S.; Kim, Y.; Infante, I.; Cho, H. Olefin Ligand Metathesis for Colloidal Emissive Nanocrystals with Enhanced Stability and Photosensitivity. *Angew. Chem. Int. Ed.* **2025**, *64*, e202514802.

[41] Lu, W.; Wu, Y.; Li, X.; Huang, J.; Ali, A.; Ren, J.; Shang, Q.; Li, C.; Baryshnikov, G. V.; Xu, B. Multifunctional Dithiol Crosslinking Additive Enables Highly Efficient and Stable Inkjet-Printed Perovskite Quantum Dot Light-Emitting Diodes. *Adv. Mater.* **2025**, *38*, e15555.

[42] Drozd, D. D.; Strokin, P. D.; Kornilov, D. A.; Drozd, A. V.; Burov, A. M.; Ushakov, A. V.; Goryacheva, O. A.; Goryacheva, I. Yu. Enhancement of the alloyed CdZnSeS/ZnS quantum dots photoluminescence by thiol ligands capping. *Chem. Eng. J.* **2024**, *492*, 152278.

[43] Jia, Y.; Li, H.; Guo, N.; Li, F.; Li, T.; Ma, H.; Zhao, Y.; Gao, H.; Wang, D.; Feng, J. et al. Long-range order enhance performance of patterned blue quantum dot light-emitting diodes. *Nat. Commun.* **2025**, *16*, 7643.

[44] Roper, T. M.; Guymon, C. A.; Jönsson, E. S.; Hoyle, C. E. Influence of the alkene structure on the mechanism and kinetics of thiol-alkene photopolymerizations with real-time infrared spectroscopy. *J. Polym. Sci. Pol. Chem.* **2004**, *42*, 6283-6298.

[45] Tian, J.; You, Y.; Zhou, H.; Li, H.; Hu, L.; Tian, Y.; Xie, H.; Xie, Y.; Hu, X. Biobased Thermoset Substrate for Flexible and Sustainable Organic Photovoltaics. *Adv. Funct. Mater.* **2024**, *34*, 2400547.

[46] Zhang, P.; Yang, G.; Li, F.; Shi, J.; Zhong, H. Direct in situ photolithography of perovskite quantum dots based on photocatalysis of lead bromide complexes. *Nat. Commun.* **2022**, *13*, 6713.

[47] Huang, G.; Zhang, F.; Xiong, X.; Sun, K.; Ruan, H.; Wang, C.; Li, C.; Zhao, Y.; Li, M.; Cheng, G. et al. Tailorable Fluorescent Perovskite Quantum Dots for Multiform Manufacturing via Two-Step Thiol-Ene Click Chemistry. *Adv. Mater.* **2025**, *37*, 2411453.

[48] Wang, S.; Yang, W.; Li, Y.; Chen, J.; Bian, Y.; Deng, J.; Hu, B.; Chen, F.; Shen, H.; Teng, F. et al. Stable and Efficient Red InP-Based QLEDs through Surface Passivation Strategies of Quantum Dots. *Nano Lett.* **2024**, *24*, 15781-15787.

[49] Huo, Y.; Luo, C.; Wu, C.; Ren, Z.; Wang, H.; Zhu, D.; Wang, L.; Zhou, X.; Zheng, Z.; Wang, X. et al. Ambient Direct Lithography Patterning of Ultra-Stable Perovskite Quantum Dots for High-Resolution Light-Emitting Diodes. *Adv. Funct. Mater.* **2025**, *35*, 2504261.

[50] Yang, J.; Lee, M.; Park, S. Y.; Park, M.; Kim, J.; Sitapure, N.; Hahm, D.; Rhee, S.; Lee, D.; Jo, H. et al. Nondestructive Photopatterning of Heavy-Metal-Free Quantum Dots. *Adv. Mater.* **2022**, *34*, 2205504.

[51] Liu, D.; Weng, K.; Zhao, H.; Wang, S.; Qiu, H.; Luo, X.; Lu, S.; Duan, L.; Bai, S.; Zhang, H. et al. Nondestructive Direct Optical Patterning of Perovskite Nanocrystals with Carbene-Based Ligand Cross-Linkers. *ACS Nano* **2024**, *18*, 6896-6907.

[52] Lu, S.; Fu, Z.; Li, F.; Weng, K.; Zhou, L.; Zhang, L.; Yang, Y.; Qiu, H.; Liu, D.; Qing, W. et al. Beyond a Linker: The Role of Photochemistry of Crosslinkers in the Direct Optical Patterning of Colloidal Nanocrystals. *Angew. Chem., Int. Edit.* **2022**, *61*, e202202633.

[53] Yang, J.; Hahm, D.; Kim, K.; Rhee, S.; Lee, M.; Kim, S.; Chang, J. H.; Park, H. W.; Lim, J.; Lee, M. et al. High-resolution patterning of colloidal quantum dots via non-destructive, light-driven ligand crosslinking. *Nat. Commun.* **2020**, *11*, 2874.

[54] Kim, J. M.; Choi, D.; Lee, N.; Chae, W. S.; Kim, H. S.; Yu, J. H.; Lee, J. S. Role of Conjugated Structure of Cross-linkers in Patterned QLEDs. *Nano Lett.* **2025**, *25*, 10435-10441.

[55] Qie, Y.; Hu, H.; Yu, K.; Zhong, C.; Ju, S.; Liu, Y.; Guo, T.; Li, F. Ligand-Nondestructive Direct Photolithography Assisted by Semiconductor Polymer Cross-Linking for High-Resolution Quantum Dot Light-Emitting Diodes. *Nano Lett.* **2024**, *24*, 1254-1260.

[56] Jing, Y.; Yao, M.; Yang, M.; Li, M.; Ding, H.; Yang, G.; Zhang, R.; Han, D.; Liu, H.; Zhong, H. Photolithographic fabrication of high-resolution Micro-QLEDs towards color-conversion microdisplay. *Light Sci. Appl.* **2025**, *14*, 370.

[57] Lin, L.; Wang, J.; Hu, H.; Luo, H.; Liu, Y.; Yang, X.; Su, J.; Li, D.; Xu, Z.; Luo, C. et al. Nanoscale transfer-printed full-colour ultrahigh-resolution quantum dot LEDs. *Nature* **2026**, *652*, 349-358.

[58] Cao, W.; Tian, S.; Zhong, C.; Qiu, L.; Zeng, P.; Chen, Z.; Zhang, X.; Liu, H.; Liu, K.; Li, J. et al. Ultrahigh-resolution nanoimprint patterning of quantum-dot light-emitting diodes via capillary self-assembly. *Nat. Photon.* **2026**, *20*, 301-309.

Electronic Supplementary Material

Robust and ultralow-energy direct photolithography of quantum dots via dual-ligand passivated thiol-ene click chemistry

Hao Tan[1,2,3], Zhixin Zhai[1,2], Chengjun Li[1,2,3], Kai Chen[1,2,3], Wenxuan Wang[1,2,3], Chang Gu[1,2,✉], Chaoyu Xiang[1,2], and Ting Zhang[1,2,✉]

[1] *Laboratory of Optoelectronic Information Technology and Devices, Ningbo Institute of Materials Technology and Engineering, Chinese Academy of Sciences, Ningbo 315201, China*
[2] *Hangzhou Bay Laboratory of Advanced Nano-Optoelectronic Materials and Devices, Qianwan Institute of CNITECH, Ningbo 315336, China*
[3] *School of Nano Science and Technology, University of Science and Technology of China, Suzhou 215123, China*

✉Address correspondence to Chang Gu, guchang@nimte.ac.cn; Ting Zhang, zhangting@nimte.ac.cn

Supporting information to https://doi.org/10.26599/NR.2026.94908915

EXPERIMENTAL METHODS

Note S1 Chemical & Materials

10-Bromo-1-decene (≥95.0%), NH4Cl (99.5%), ethyl acetate (≥99.5%), methyl acetate (≥99%), 1-dodecanethiol (≥98%), pentaerythritol tetra(3-mercaptopropionate) (>90.0%), 1,10-decanedithiol (96%), 1,8-octanedithiol (≥98%) and 1,6-hexanedithiol (≥97%) were purchased from Aladdin Reagent Company. Potassium thioacetate (98%), lithium aluminum hydride, tetrahydrofuran (THF, 99.5%, Extra Dry), pentaerythritol tetrakis(mercaptoacetate) (94%), poly(methyl methacrylate) (PMMA, 97%) and MgSO4 (99%) were obtained from Energy Chemical (3A) Company. Acetone (≥99.5%), dichloromethane (≥99.5%) and toluene (≥99.5%) were obtained from Sinopharm Chemical Reagent Co., Ltd. 1,4-Butanediol bis(thioglycolate) (≥95%) was purchased from Macklin Reagent Company. Thermal-cured poly(9,9-dioctylfluorenyl-2,7-diyl)-co-(4,4'-(N-(p-butylphenyl))diphenylamine) (X1-TFB) was purchased from Volt-Amp Optoelectronics Tech. Co. Ltd. Poly(3,4-ethylenedioxythiophene): poly(styrenesulfonate) (PEDOT: PSS, AI 4083) was purchased from Xi'an Polymer Light Technology Co.

Commercial red core-shell CdSe/ZnS QDs (20 mg/mL in toluene; PL peak position at 627 nm or 622 nm), green core-shell CdSe/ZnS QDs (20 mg/mL in toluene; PL peak position at 537 nm), green core-shell InP/ZnSe/ZnS QDs (20 mg/mL in toluene; PL peak position at 534 nm), blue core-shell CdZnSe/ZnSe/ZnS QDs (20 mg/mL in toluene; PL peak position at 471 nm or 481 nm) and ZnO nanoparticles (30 mg/mL in ethanol) were provided by Hefei Full-Nano Co. Ltd.

ITO (30 Ω sq^{-1}) was obtained from Huayi Electronic Co., Ltd. and Liaoning Advanced Election Technology. ITO was cleaned with deionized water, acetone and isopropanol for 15 min, and then exposed under UV Ozone for 15 min before use.

Note S2 Instrument characterization

UV-vis absorption spectra were measured using a Shimadzu UV-2600i double-beam spectrophotometer. PL spectra were performed using FluoroMax Plus (HORIBA). The lifetime of QDs was measured by Fluorolog-QM (HORIBA). PL QYs were measured by an absolute PL QY spectrometer (C9920-02, Hamamatsu). The size distribution of QDs was measured by Zetasizer ultra (Malvern Panalytical). ^{1}H NMR was performed using AVANCE NEO 400M (Bruker). Thermogravimetric analysis (TGA) data of QDs was collected using a NETZSCH TGA209F1 instrument at a heating rate of 10 °C min^{-1} under nitrogen flow. The morphology was observed with Bruker DIMENSION Icon (AFM). Ultraviolet photoelectron spectroscopy (UPS) and X-ray photoelectron spectroscopy (XPS) were performed using an AXIS SUPRA+. Fourier transform infrared (FT-IR) spectra were performed using a IS50 (Thermo Fisher Scientific). Grazing-incidence small-angle X-ray scattering (GISAXS) measurements were performed using the Xeuss 3.0 UHR instrument (Xenocs, France) with an incident angle of 0.2°, Cu-Kα radiation wavelength of 1.54 Å, and a sample-to-detector distance of 500 mm equipped with an Eiger 500K detector.

Direct photolithography was performed with UV LED lamps (centered at 254 nm, ~0.5 or ~5 mW/cm^2) from Zigu Factory, Zhongshan, China. The power density was measured by LS125 with LS125-UVC-X0 Probe from Linshang Technology, Shenzhen, China. Functional materials were coated on the substrate by EZ4 SPIN COATER (Schwan technology). Images of patterned QDs and QLEDs were obtained on a fluorescence microscope (Olympus BX51 with DP74 camera). CS-2000 (Konica Minolta) and Keithley 2400 B were applied to measure the luminance and current density of QLEDs, respectively.

Note S3 Synthesis of dec-9-ene-1-thiol

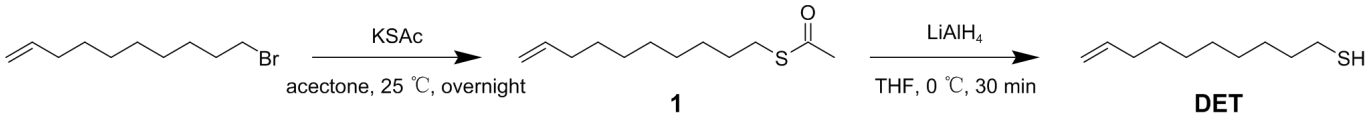

The synthesis method described herein was primarily based on the literature procedure with some modifications (Ref. S1). Potassium thioacetate (KSAc, 3.38 g, 29.59 mmol), 10-bromo-1-decene (5.46 g, 24.91 mmol), and acetone (50 mL) were placed into a round bottom flask. The reaction mixture was stirred at 25 °C overnight under a nitrogen atmosphere. Then, the mixture was washed by a saturated aqueous solution of ammonium chloride and dichloromethane (DCM). The combined organic phases were dried over an adequate amount of anhydrous magnesium sulfate, followed by filtration. The solvent was subsequently removed by vacuum, and the intermediate product (**1**) (yellow oil, yield = 75.8%) was obtained. 1H NMR (400 MHz, Chloroform-d) δ 5.88 - 5.74 (m, 1H), 5.04 - 4.90 (m, 2H), 2.86 (t, 2H), 2.32 (s, 3H), 2.04 (q, J = 6.9 Hz, 2H), 1.56 (p, J = 7.2 Hz, 2H), 1.41 - 1.32 (m, 4H), 1.28 (m, 6H). ^{1}H-NMR was shown in Fig. S3.

The intermediate product 1 (649 mg, 3.03 mmol) and 10 mL of tetrahydrofuran (THF) were placed into a round bottom flask. The mixture was stirred continuously at 0 °C (maintained with an ice-water bath). A solution of lithium aluminum hydride ($LiAlH_4$) in THF (2.5 mmol/mL, 1.6 mL) was added dropwise slowly to the reaction flask and then stirred for 30 minutes. Then, the reaction was quenched by the dropwise addition of an aqueous solution of sodium hydrogen sulfate. The resulting mixture was washed by ethyl acetate and a saturated aqueous solution of ammonium chloride. The combined organic phases were dried over an adequate amount of anhydrous magnesium sulfate until the solution became clear, followed by filtration. The solvent was removed by vacuum, and the product (**DET**) (yellow oil, yield = 71.2%) was obtained. 1H NMR (400 MHz, Chloroform-d) δ 5.88 - 5.74 (m, 1H), 5.04 - 4.90 (m, 2H), 2.52 (q, J = 7.4 Hz, 2H), 2.04 (q, J = 7.0 Hz, 3H), 1.61 (p, J = 7.2 Hz, 2H), 1.37 (m, 4H), 1.33 (s, 1H), 1.30 (m, 6H). ^{1}H-NMR was shown in Fig. S3.

Note S4 Ligand exchange

3 mL of a 20 mg/mL OA-capped QD solution was combined with 9 mL of 1-dodecanethiol in a reaction flask and stirred at 80 °C under a nitrogen atmosphere for 2 hours. The reaction solution was then transferred to a centrifuge tube, mixed with methyl acetate, and centrifuged at 8000 rpm for 3 minutes. The precipitate was re-dissolved in toluene. The above ligand exchange process was repeated once again to replace OA ligands as much as possible. Then, the as-prepared QDs was washed with methyl acetate for two times to remove additional free ligands. Finally, the QD solution was diluted with toluene to a 20 mg/mL QD solution.

1 mL of the 20 mg/mL QD solution was transferred to a centrifuge tube and mixed with 2 mL of methyl acetate. The mixture was centrifuged at 8000 rpm for 3 minutes. Subsequently, an appropriate amount of toluene was added to dissolve the QDs, followed by the addition of 2 mg of dec-9-ene-1-thiol (DET) to passivate QD surface defects. Finally, the QD solution was diluted with toluene to a 20 mg/mL QD solution (designated as DLP-QD, toluene).

Owing to the high reactivity of the C=C bond in the DET ligand, which made it susceptible to chemical deterioration at elevated temperatures, we avoided using a one-step ligand exchange procedure.

Note S5 The calculation details of the content distribution of ligands in DLP-QDs

$$C_{DET}=\beta/(\alpha+\gamma)$$

$$C_{1\text{-}DT}=(\alpha-\beta)/(\alpha+\gamma)$$

$$C_{OA}=\gamma/(\alpha+\gamma)$$

C_{DET}, $C_{1\text{-}DT}$ and C_{OA} denote the content of DET, 1-DT and OA ligands in DLP-QDs, respectively. And α, β, and γ represent the integrated areas at characteristic peak positions indicated in Fig. S4. The calculation results were summarized in Table S1.

Note S6 The calculation details of the ligand densities of QDs

The calculation formula for ligand density is shown below:

$$Ligand\ Density=\frac{\frac{m_x}{M_x}\times N_A}{S}=\frac{\frac{m_x}{M_x}\times N_A}{V\times\frac{6}{d}}=\frac{\rho d W_x N_A}{6M_x}$$

where m_x, M_x, N_A, S, V, d, ρ and W_x represent the mass of different ligands, their molar mass, Avogadro's constant (6.02×10^{23} mol^{-1}), the total surface area of the core- shell QDs, the total volume of the core- shell QDs, the diameter of the QDs, the density of the core- shell QDs and the mass ratio of each ligand to the core- shell QDs (determined by TGA), respectively. The molar masses of OA, 1- DT, and DET are 282.5, 202.4, and 172.3 g mol^{-1}, respectively. The mass ratios of ligand to the core-shell QDs were obtained from thermogravimetric analysis measurements, as shown in Fig. S6. The diameter of the QDs was consistent with reported values in our recent work (Ref. S2), approximately 10.9 nm.

To obtain the density of the core-shell QDs, we performed the corresponding calculations. The CdSe core size of the QDs was estimated from UV-visible absorption spectra using the equation $d_{CdSe} = 1280/(810 - \lambda) - 1.9$, where λ represents the wavelength of the first excitonic absorption peak of the QDs (Ref. S3). The diameter of the CdSe core was calculated to be 4.9 nm. Furthermore, the densities of zinc-blende CdSe and ZnS were obtained from the CRC Handbook of Chemistry and Physics, being 5.81 and 4.04 g cm^{-3}, respectively. The density of the core-shell QDs was calculated using the following formula:

$$\rho = \frac{\rho_{CdSe} V_{CdSe} + \rho_{ZnS} V_{ZnS}}{V_{CdSe} + V_{ZnS}}$$

The density of the core-shell QDs was 4.20 g cm^{-3}. From these, one can calculate the ligand densities, as listed in Table S3.

Note S7 Direct photolithography of QDs

Red DLP-QD and pentaerythritol tetra(3-mercaptopropionate) (PTMP) were taken as a typical example to introduce the direct photolithography of QDs. The blending content of PTMP defaults to 10 wt% of DLP-QD. At first, the blended solution was spin-coated on a cleaned silicon or other substrates at 2000 rpm to form a DLP-QD/PTMP film. And then the film was exposed to UV lamps (centered at 254 nm, ~0.5 or ~5 mW/cm^2) with different photomasks for required patterns in a nitrogen-filled glove box. After UV exposure, the film was spin-coated with toluene to wash off the un-crosslinked areas.

In a typical patterning procedure for red/green/blue-emitting DLP-QDs, the PTMP content and exposure dose were optimized as follows: 10 wt% with ~10 mJ/cm^2 for red, 5 wt% with ~1 mJ/cm^2 for green, and 5 wt% with ~2 mJ/cm^2 for blue. For QLEDs based on patterned red DLP-QDs, a PTMP content of 1 wt% and an exposure dose of ~40 mJ/cm^2 were employed. For QLEDs based on patterned green and blue DLP-QDs, the required PTMP content and exposure dose were identical to those employed for their respective optical patterning.

Note S8 The definition and calculation details of film maintenance ratio

The film maintenance ratio is defined as the ratio of the thickness of the QD film after exposure and development processes to its initial film thickness. And the film thickness was determined by measuring the surface profile with AFM and calculating the height difference between the undisturbed regions and the regions where the film had been removed. The film maintenance ratio is calculated by following equations:

$$\textit{Film maintenance ratio} = \frac{\textit{Thickness of the QD film after exposure and development}}{\textit{Thickness of the initial QD film}}$$

The measurements were performed in triplicate to eliminate stochastic errors. The resulting data were presented with error bars incorporated into the relevant figures to reflect measurement variability and enhance data reliability.

Note S9 Nanoparticle size distribution

The mean centre-to-centre distance (d) for neighboring QDs is calculated from the peak position in the GISAXS scattering profile using the equation (Ref. S4):

$$d = 2\pi/q$$

According to the GISAXS data shown in Fig. S16, the d of DLP-QD film and DLP-QD/PTMP film after UV exposure is 13.61 nm and 13.98 nm, respectively.

Note S10 Preparation of QLEDs

We take the red QLED based on photolithographic DLP-QD as a typical example to introduce the preparation process. At first, PEDOT: PSS (AI 4083) was spin-coated on a cleaned ITO substrate at 3000 rpm, followed by annealing at 150 °C for 15 min in air. Then, X1-TFB (8 mg/mL in chlorobenzene) was spin-coated at 1500 rpm and crosslinked at 200 °C for 30 min. Subsequently, an appropriate amount of toluene solution was spin-coated at 1500 rpm to remove un-crosslinked components and annealed at 150 °C for 5 min.

After that, for the non-patterned QLED, the pristine QD or photolithographic DLP-QD film (non-patterned) was prepared as described above. The entire DLP-QD layer was exposed to UV lamps (centered at 254 nm, ~5 mW/cm^2) for crosslinked DLP-QD film. Here, the blending content of PTMP defaults to 1 wt% of DLP-QD. After UV expose, the film was spin-coated with toluene at 2000 rpm and annealed at 80 °C for 5 min. For the patterned QLED, the pristine QD or patterned DLP-QD film was prepared as described above. The red DLP-QD layer was exposed to UV lamps (centered at 254 nm, ~0.5 mW/cm^2) with different photomasks for patterned red DLP-QD film. Subsequently, PMMA (2 mg/mL in acetone) was spin-coated at 5000 rpm and annealed at 60 °C for 30 min.

Then, ZnO nanoparticles (30 mg/mL in ethanol) was spin-coated at 2000 rpm and annealed at 80 °C for 30 min. And a silver (Ag) layer was deposited as the electrode by using vapor deposition (thickness: 150 nm). Finally, the QLED was encapsulated to isolate water and oxygen from the air.

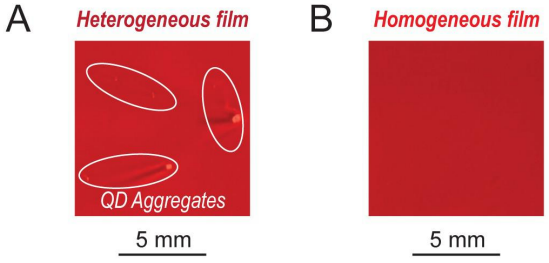

Figure S1 Fluorescence photos of the spin-coated OA-QD/PTMP film (A) and DLP-QD/PTMP film (B).

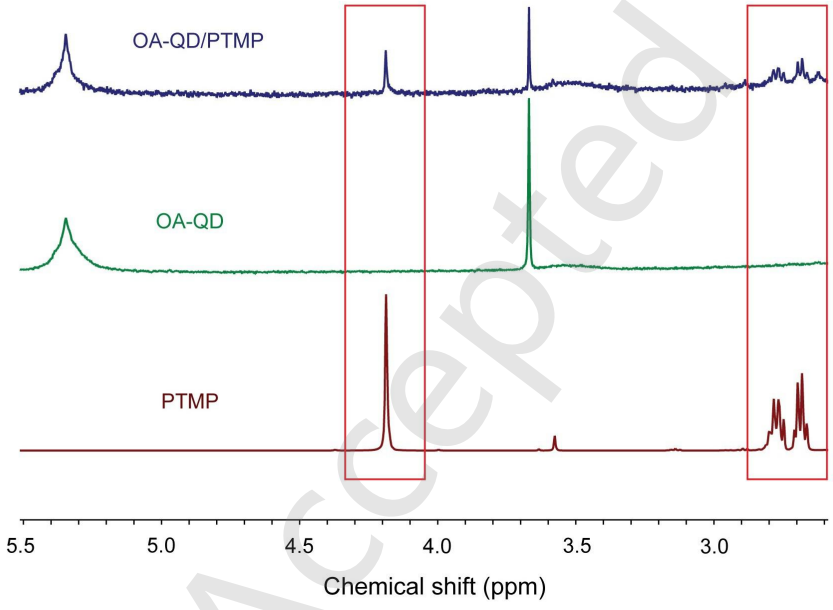

Figure S2 ^{1}H-NMR (400 MHz, Chloroform-d) of PTMP, OA-QD and OA-QD/PTMP.

Note: For OA-QD/PTMP, the fresh mixture was stored for 10 minutes, followed by washing with methyl acetate twice to remove free ligands and unanchored PTMP before NMR analysis to prevent errors.

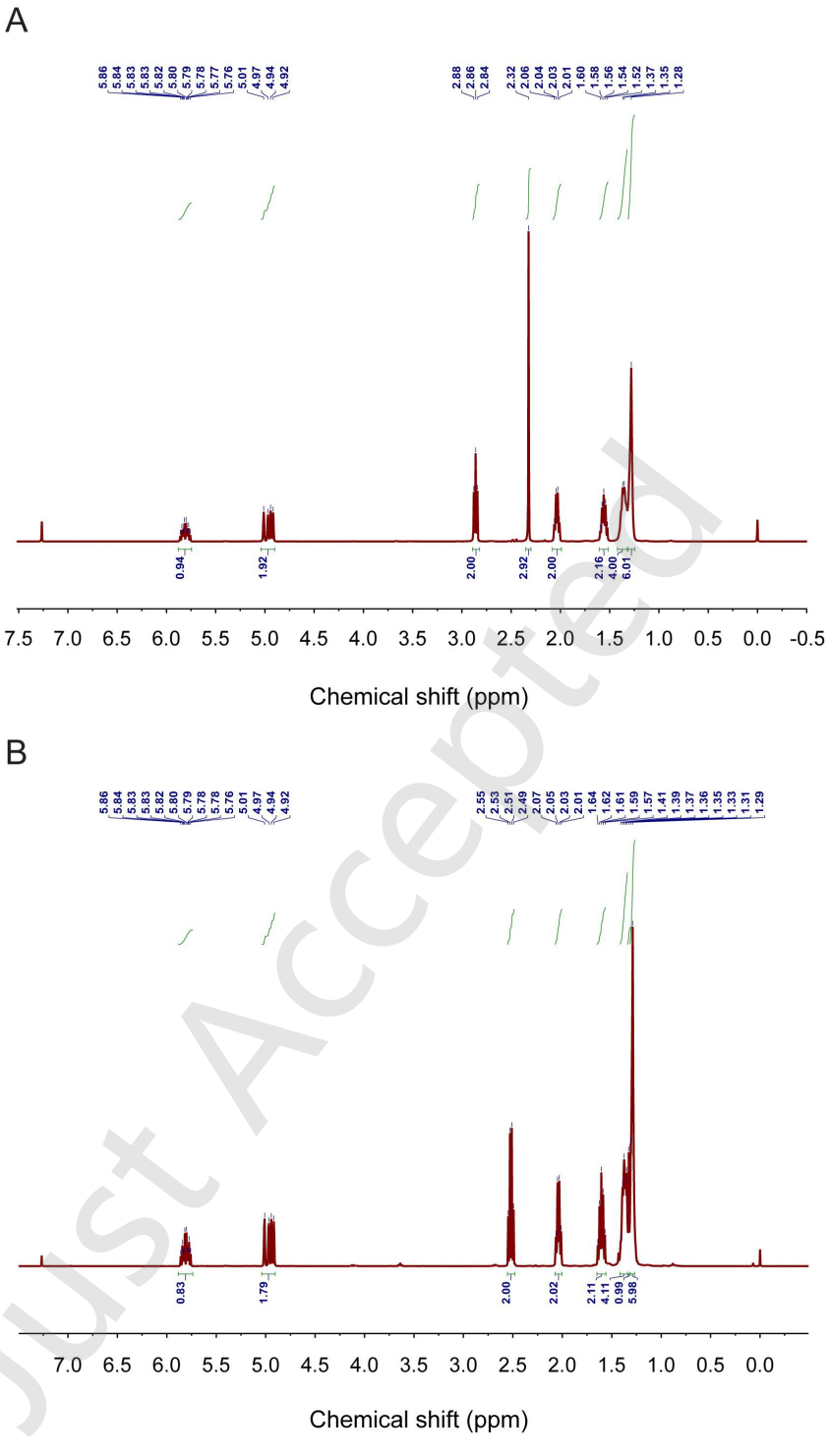

Figure S3 ^{1}H-NMR (400 MHz, Chloroform-d) of 1 (A) and DET (B).

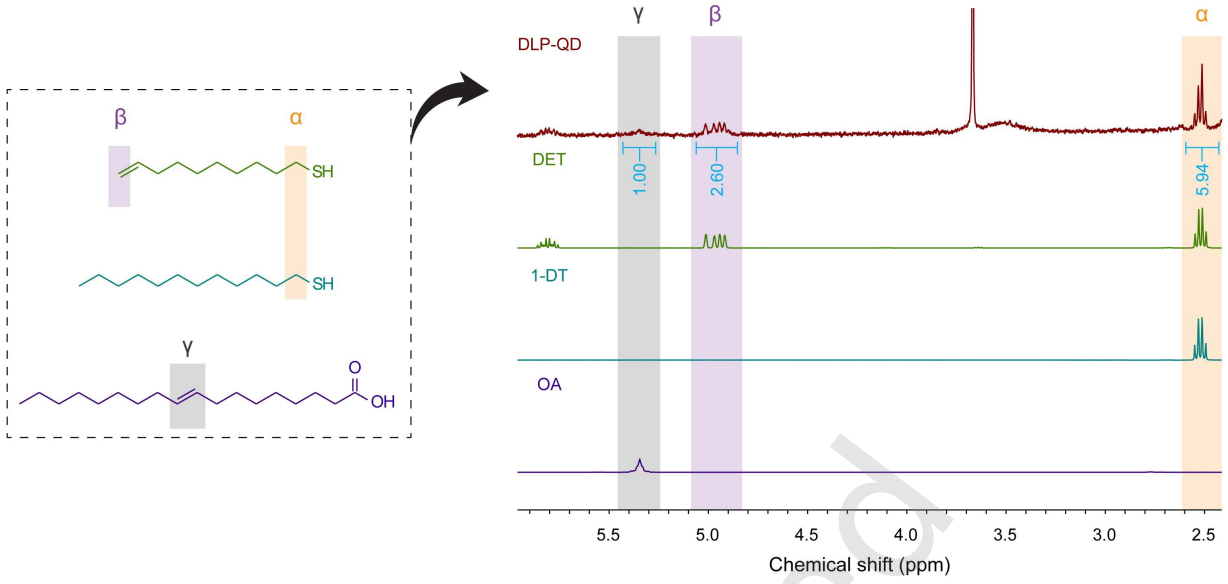

Figure S4 ^{1}H-NMR (400 MHz, Chloroform-d) of DLP-QD, DET, 1-DT and OA.

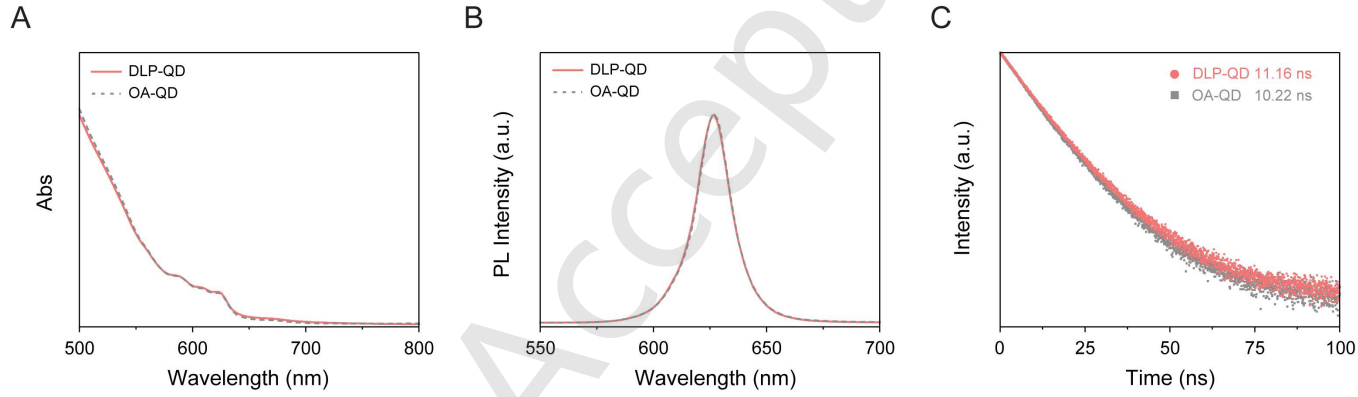

Figure S5 UV-vis absorption spectra (A) and PL spectra (B) of OA-QD and DLP-QD solution. (C) PL decay curves of OA-QD and DLP-QD films.

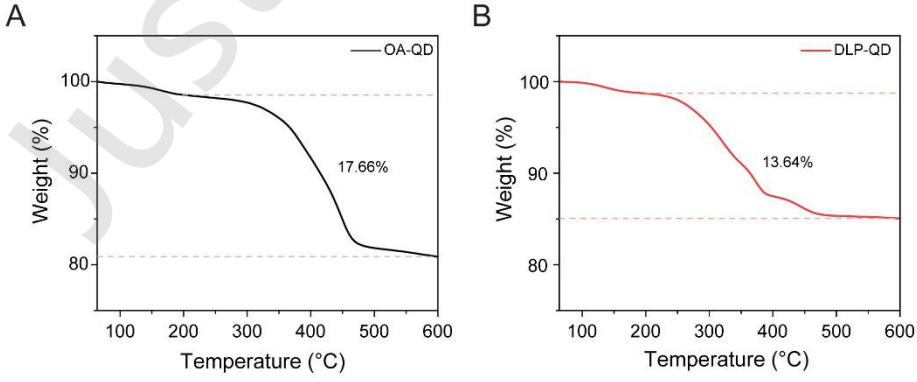

Figure S6 Thermogravimetric analysis measurement of OA-QD (A) and DLP-QD (B). The weight loss below 200 ℃ corresponds to solvent evaporation.

Figure S7 Photo of DLP-QD/PTMP solution after 120-days storage.

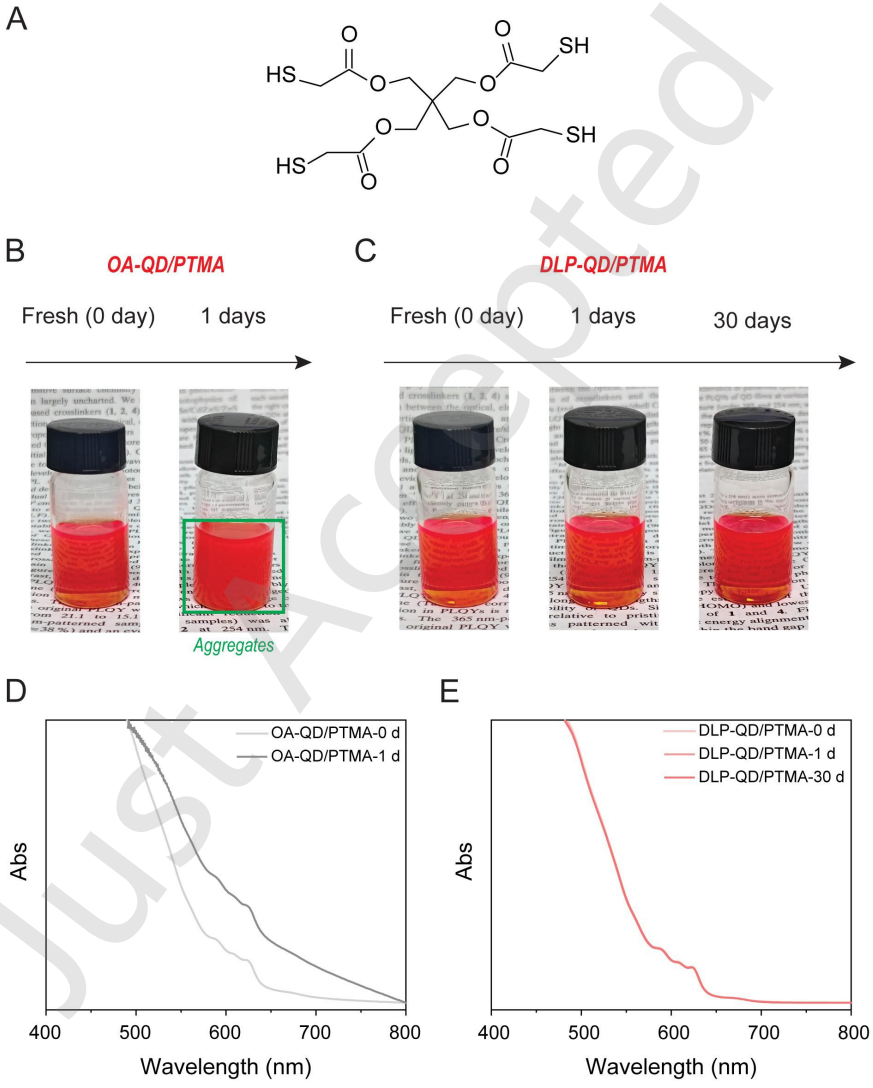

Figure S8 (A) Molecular formula of PTMA. Photos of OA-QD/PTMA solution (B) and DLP-QD/PTMA solution (C) for different days. UV-vis absorption spectra of OA-QD/PTMA (D) and DLP-QD/PTMA (E) for different days.

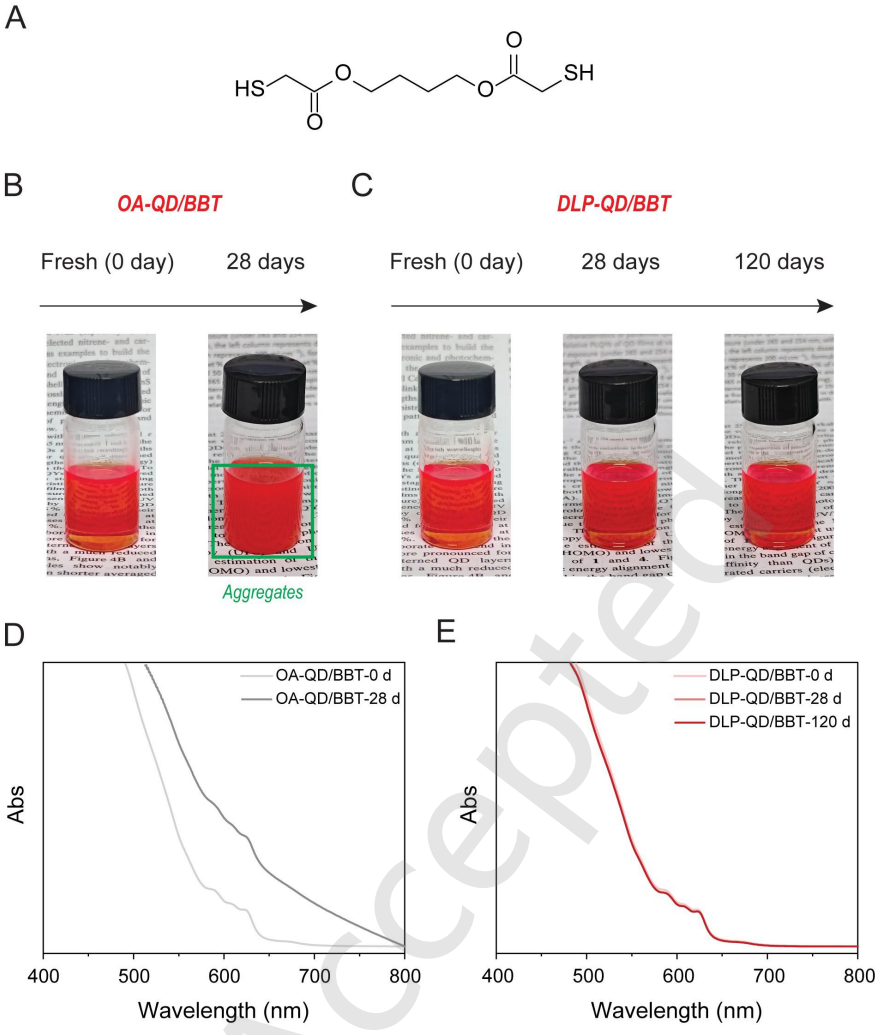

Figure S9 (A) Molecular formula of BBT. Photos of OA-QD/BBT solution (B) and DLP-QD/BBT solution (C) for different days. UV-vis absorption spectra of OA-QD/BBT (D) and DLP-QD/BBT (E) for different days.

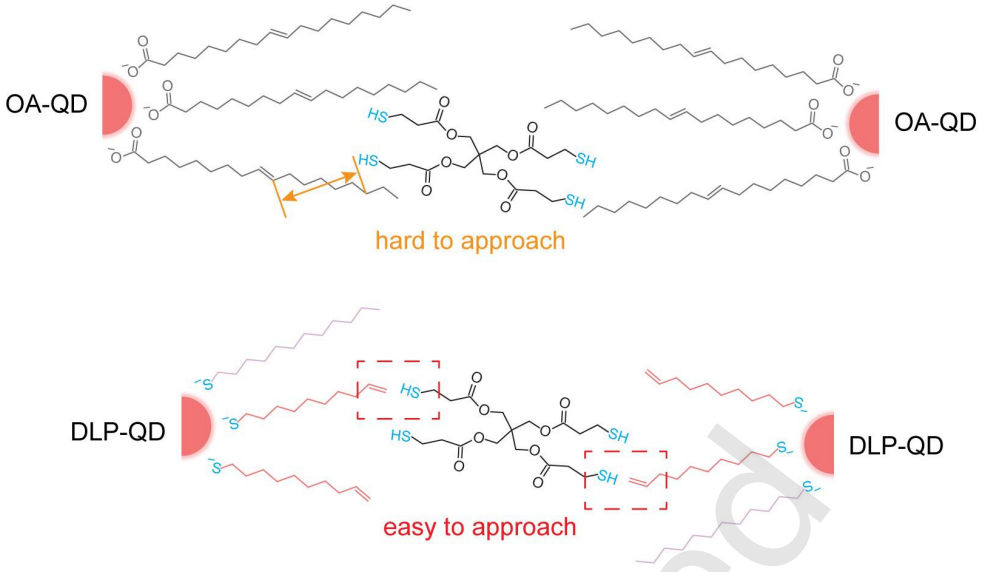

Figure S10 Schematic of spatial distribution of OA-QD and DLP-QD with PTMP.

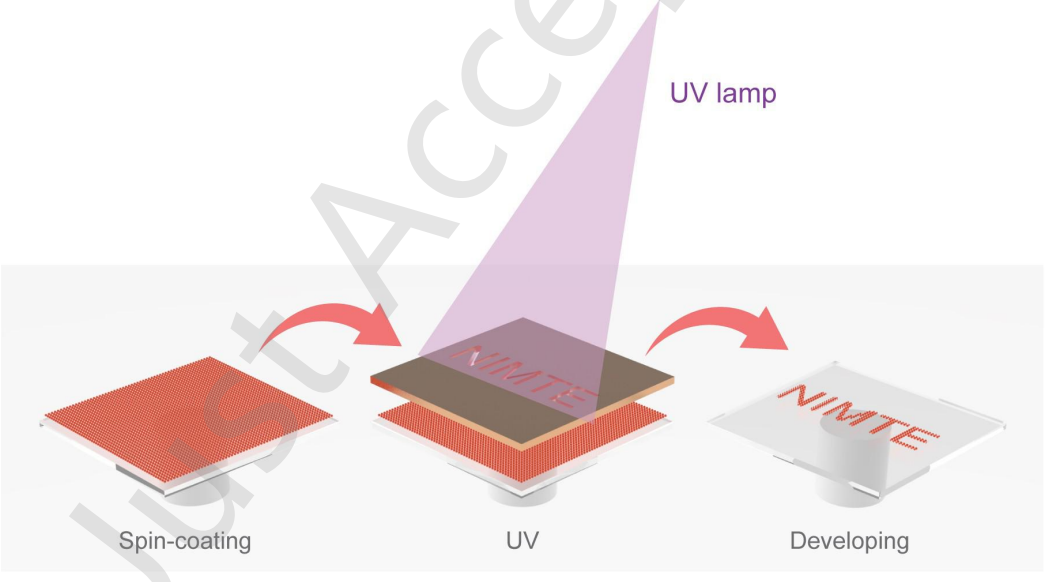

Figure S11 Schematic of direct photolithography of QDs.

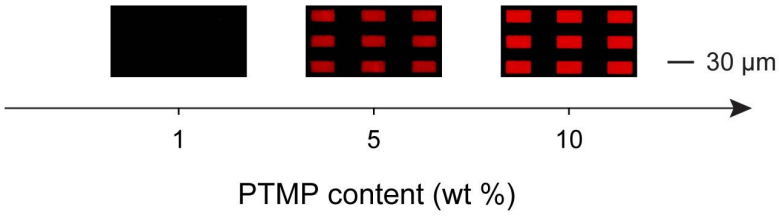

Figure S12 Fluorescence microscopic images of photolithographic DLP-QD patterns with various contents of PTMP at 10 mJ/cm^2. The same photomask as in Fig. 2b was used.

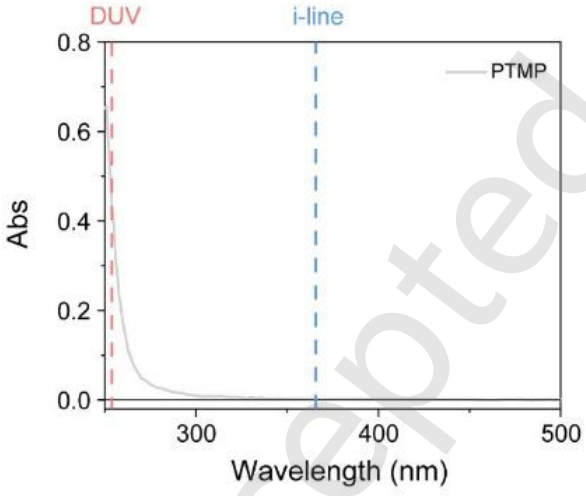

Figure S13 UV-vis absorption spectrum of PTMP solution in CH_2Cl_2 (2 mg/mL).

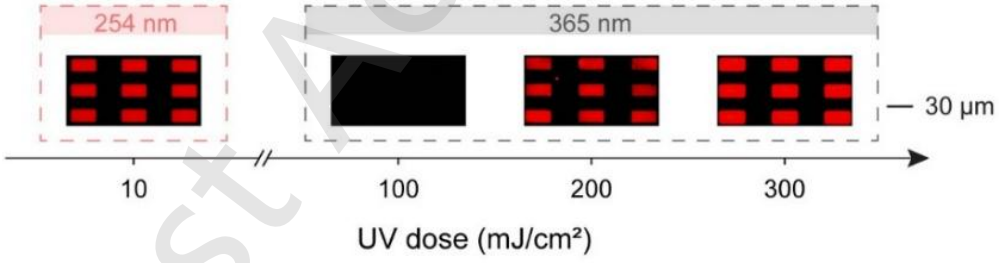

Figure S14 Fluorescence microscopic images of photolithographic DLP-QD patterns in different wavelengths and UV doses with the same blending content of PTMP (10 wt% of DLP-QD). The same photomask as in Fig. 2b was used.

Figure S15 Fluorescence microscopic image of photolithographic DLP-QD pattern at 30 mJ/cm^2 without PTMP. The same photomask as in Fig. 2b was used.

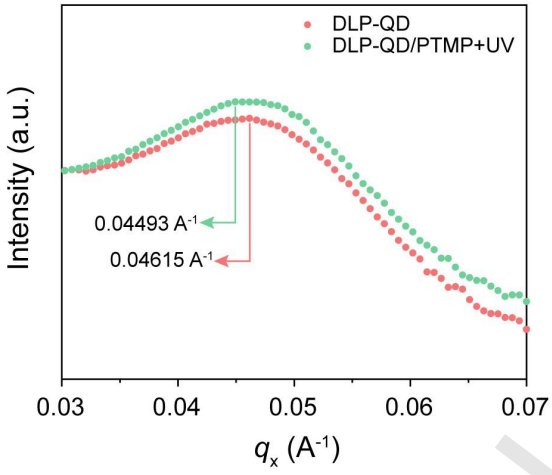

Figure S16 GISAXS spectra showing the interparticle distance of the DLP-QD film (red) and DLP-QD/PTMP film after UV exposure (green).

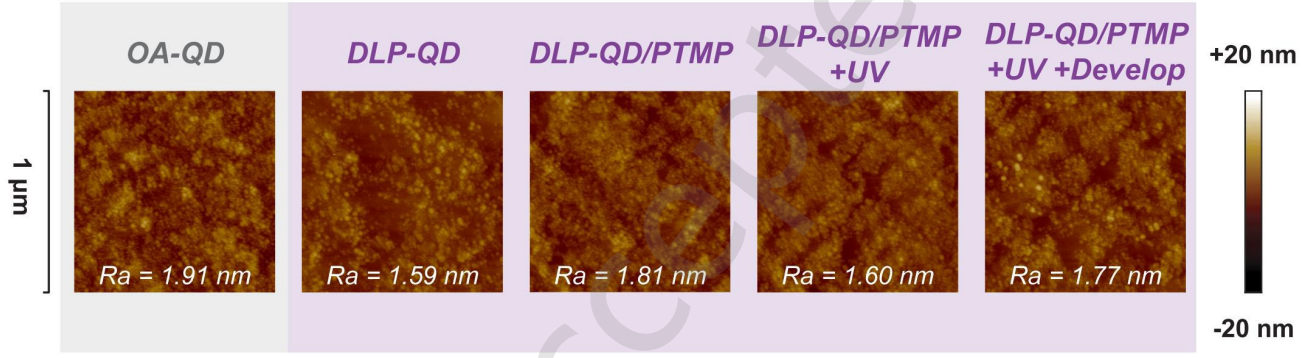

Figure S17 AFM images of OA-QD film, DLP-QD film, DLP-QD/PTMP film, DLP-QD/PTMP film after UV exposure and DLP-QD/PTMP film after UV exposure and developing.

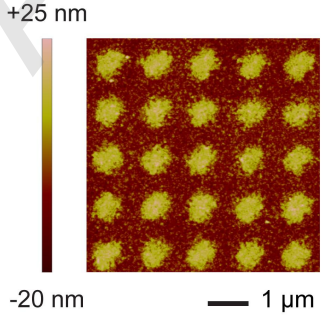

Figure S18 AFM image of pixel arrays of patterned DLP-QDs.

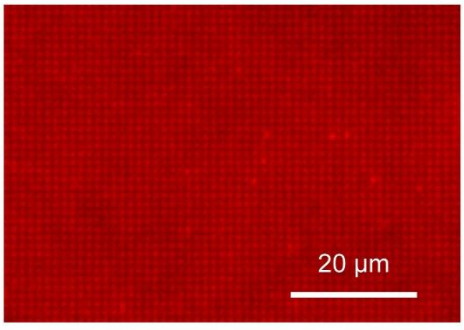

Fig. S19 Fluorescence microscopic image of photolithographic pixel array of OA-QD through PTMP (UV dose = 100 mJ/cm^2).

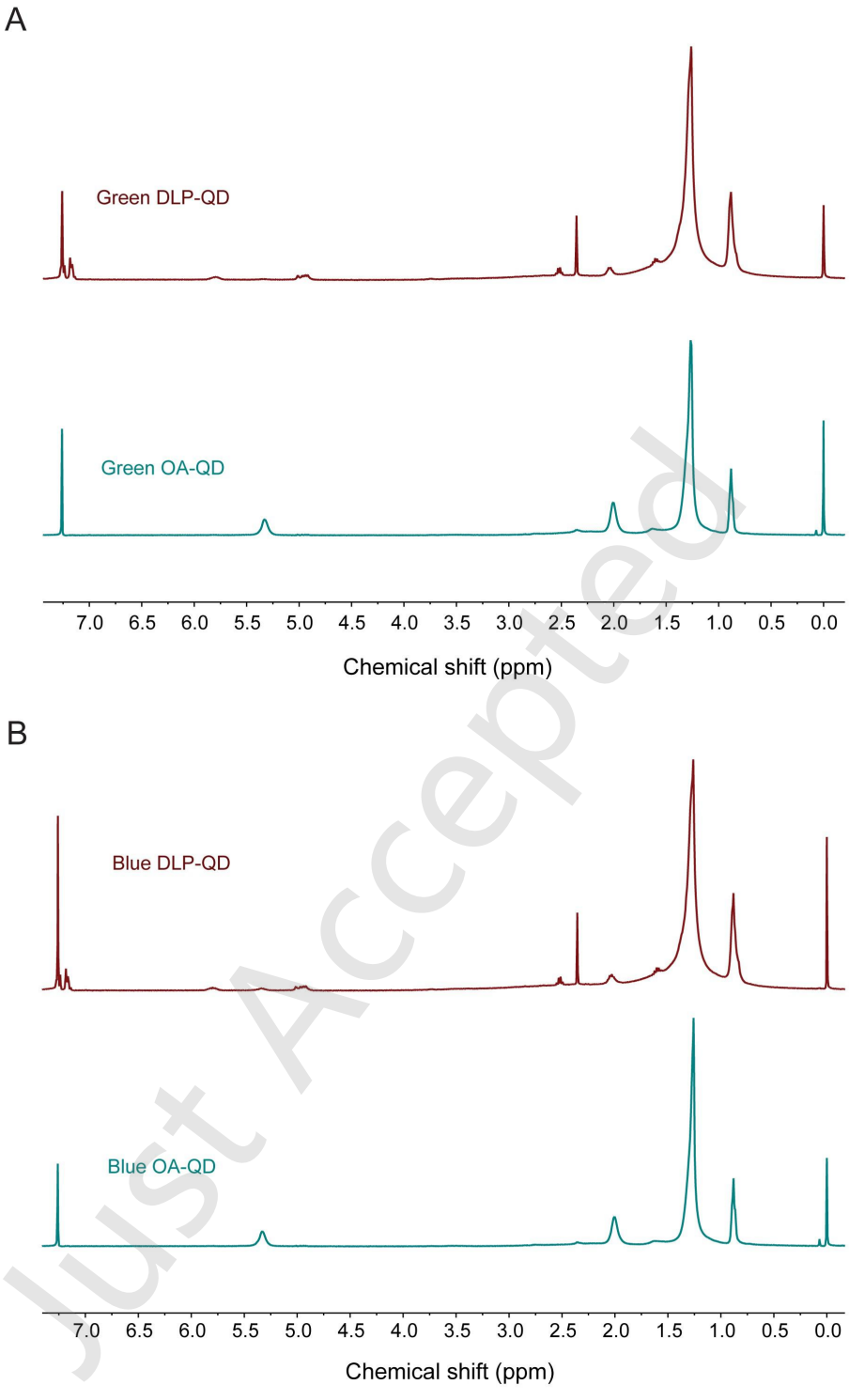

Figure S20 (A) ^{1}H-NMR (400 MHz, Chloroform-d) of green OA-QD and green DLP-QD. (B) 1H-NMR (400 MHz, Chloroform-d) of blue OA-QD and blue DLP-QD.

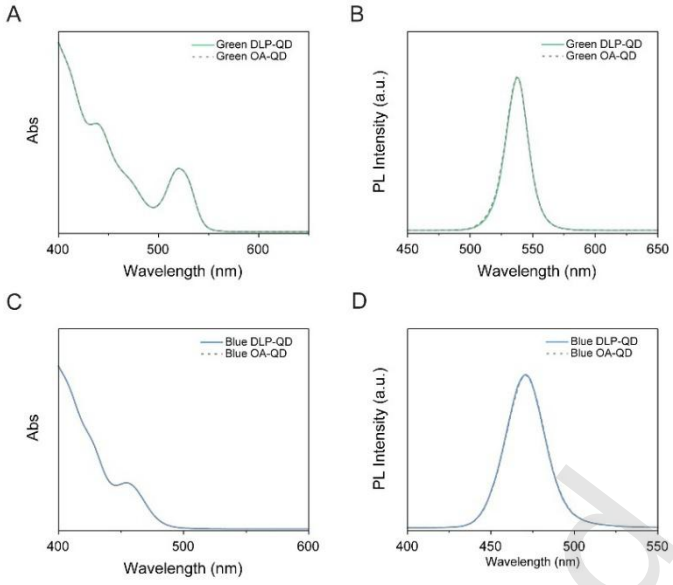

Figure S21 UV-vis absorption spectra (A) and PL spectra (B) of Green DLP-QD and OA-QD solution. UV-vis absorption spectra (C) and PL spectra (D) of Blue DLP-QD and OA-QD solution.

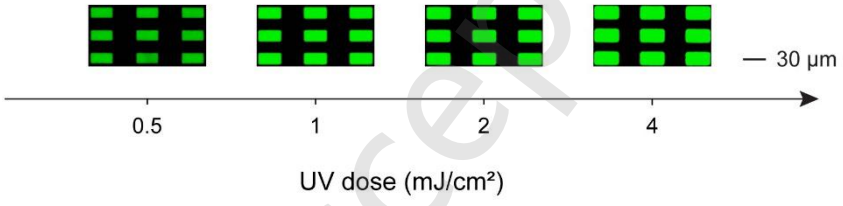

Figure S22 Fluorescence microscopic images of photolithographic Green DLP-QD patterns with various UV doses. The same photomask as in Fig. 2b was used.

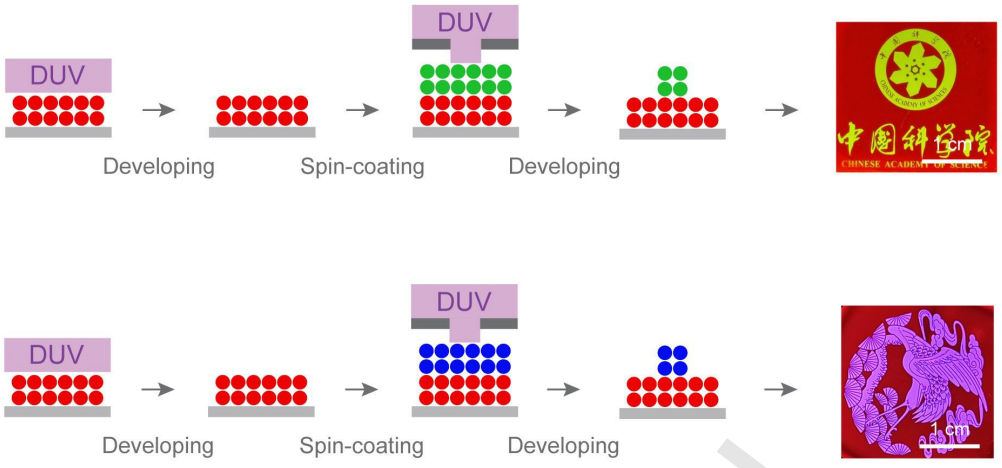

Figure S23 Schematic of vertical stacking of QD patterns.

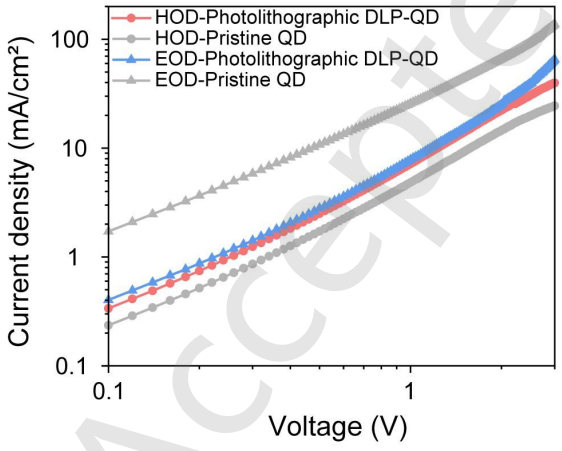

Figure S24 Current density-voltage characteristics of HODs and EODs implementing pristine QD and photolithographic DLP-QD.

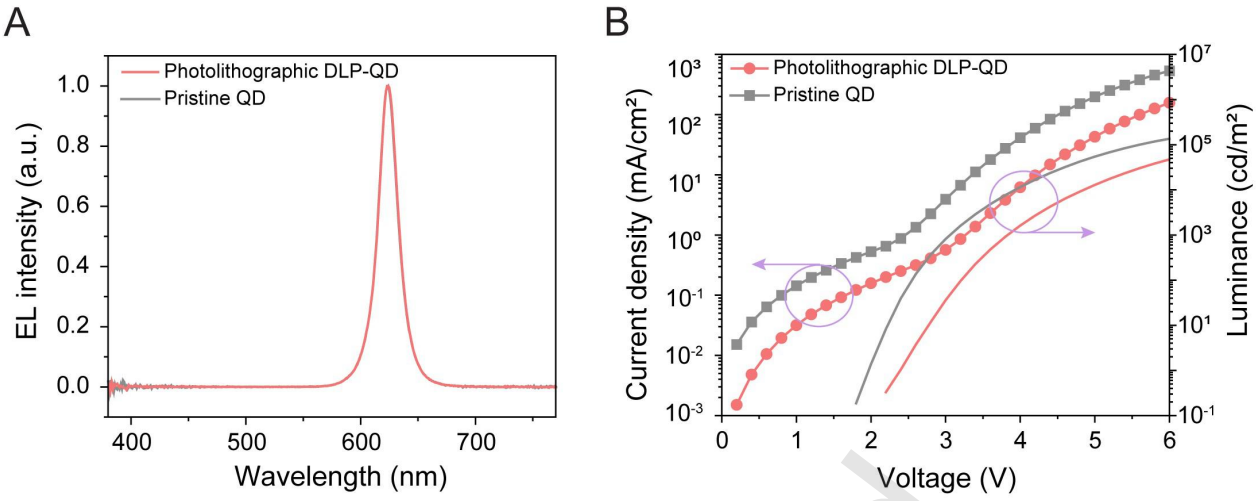

Figure S25 (A) EL spectra of QLEDs based on pristine QD and photolithographic DLP-QD. (B) Current density-voltage-luminance characteristics of QLEDs implementing pristine QD and photolithographic DLP-QD.

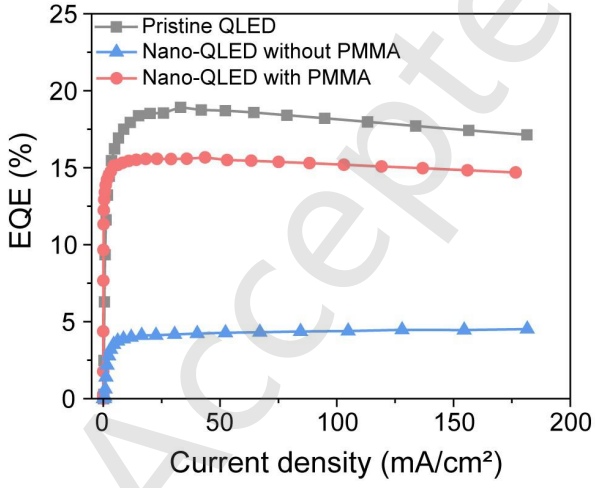

Figure S26 Current density dependent EQEs of pristine QLED, Nano-QLED without PMMA, and Nano-QLED with PMMA.

Table S1 The content distribution of ligands in DLP-QDs.

Ligand type	**DET**	**1-DT**	**OA**
Content (%)	37	49	14

Table S2 Fitting results of PL decay curves.

Sample	τ_1***(ns)***	τ_2***(ns)***	A_1 ***(%)***	A_2 ***(%)***	τ_{avg} ***(ns)***
OA-QD	6.76	13.24	63.03	36.97	**10.22**
DLP-QD	8.21	15.69	74.60	25.40	**11.16**

Table S3 The ligand densities of OA-QD and DLP-QD.

QD type	**OA-QD**	**DLP-QD**		
Ligand type	**OA**	**DET**	**1-DT**	**OA**
Ligand density (nm^{-2})	**3.55**	**1.35**	**1.78**	**0.51**

Table S4 The performance of PL pixels based on photolithographic QDs or perovskites and EL devices fabricated via photolithography.

Ref.	*QDs or perovskites*	*Patterning approach*		*UV dose (mJ/cm²)*	*PL pixel resolution (μm)*	*EQE (non-patterned QLED)*	*EQE (patterned QLED) and pixel size/line width*
This work	**CdSe/ZnS**	**Thiol-ene**	**PTMP+ DET**	**~1**	**~0.77**	**21.17%**	**15.67% and 0.80 μm**
S3	CdZnSe/CdZnS/ZnS	Nitrene and carbene C-H insertion reaction		20	3	12.6%	-
S4	InP/ZnSe/ZnS	Thiol-ene	PTMP+ OA	18000	5	-	-
S5	$CsPbBr_3$		PTMP+ OAm	~30	≥0.56	-	~3% and ~3 μm
S6	$CsPbBr_3$		ODT/DDT +OA/OAm	120	1	14.7%	-
S7	$CsPbBr_3$		DE+VPA	20	2.5	-	13.09% and 10 μm
S8	CdZnSe/ZnS/ CdZnS		BPDT/TBBT+ OA	3600	2	-	9.73% and 20 μm
S9	InP/ZnSeS	Nitrene C-H insertion reaction		2	1	8.3%	-
S10	CdSe/CdZnS	Nitrene C-H insertion reaction		2	~2	14.6%	-
S11	$FAPbBr_3$	Carbene C-H insertion reaction		35	~2	16%	-
S12	CdSe/ZnS	DMPA+TFB polymer crosslinking reaction		1200	1.5	-	16.25% and 1.5 μm
S13	CdZnSe/ZnS/ CdZnS	Carbene C-H insertion reaction		1000	~2	10.3%	9.5% and ~10 μm
S14	CdSe/ZnS	Radical-induced photopolymerization		75	1	22.0%	-
S15	CdSe	Nitrene C-H insertion reaction		20	1	-	21.08% and 500 μm
S16	CdSe/ZnS	Oxygen-mediated photochemical reactions		40	1	20.2%	-
S17	Green perovskite	Conventional photolithography		-			10.8% and 0.89 μm
S18	CdZnSe/CdZnS/ZnS	Conventional photolithography		-			13.7% and 2 μm

References

[S1] Yang, Z.; Yang, C.; Chen, S.; Chen, X.; Zhang, L.; Ren, H. Catalyst free annulative thioboration of unfunctionalized olefins. *Chem. Commun.* **2017**, *53*, 12092-12095.

[S2] Gu, C.; Zhai, Z.; Wang, W.; Tan, H.; Ding, S.; Fan, J.; Qian, L.; Zhang, T.; Xiang, C. Ultra-high-resolution nondestructive photolithography of quantum dots enabled by photo-shield crosslinker. *Mater. Today* **2025**, *89*, 100-106.

[S3] Lu, S.; Fu, Z.; Li, F.; Weng, K.; Zhou, L.; Zhang, L.; Yang, Y.; Qiu, H.; Liu, D.; Qing, W. et al. Beyond a Linker: The Role of Photochemistry of Crosslinkers in the Direct Optical Patterning of Colloidal Nanocrystals. *Angew. Chem., Int. Edit.* **2022**, *61*, e202202633.

[S4] Shin, S.; Kang, K.; Jang, H.; Gwak, N.; Kim, S.; Kim, T. A.; Oh, N. Ligand-Crosslinking Strategy for Efficient Quantum Dot Light-Emitting Diodes via Thiol-Ene Click Chemistry. *Small Methods* **2023**, *7*, 2300206.

[S5] Maeng, S.; Park, S. J.; Lee, J.; Lee, H.; Choi, J.; Kang, J. K.; Cho, H. Direct photocatalytic patterning of colloidal emissive nanomaterials. *Sci. Adv.* **2023**, *9*, eadi6950.

[S6] Maeng, S.; Kim, J.; Kim, T.; Lee, S.; Han, S.; Park, S. J.; Kim, C.; Kim, J.; Lee, J. Y.; Cho, H. Dual-Strategy Direct Photocatalytic Patterning for Efficient Perovskite Nanocrystal LED Displays. *Adv. Mater.* **2025**, *37*, e08217.

[S7] Huo, Y.; Luo, C.; Wu, C.; Ren, Z.; Wang, H.; Zhu, D.; Wang, L.; Zhou, X.; Zheng, Z.; Wang, X. et al. Ambient Direct Lithography Patterning of Ultra-Stable Perovskite Quantum Dots for High-Resolution Light-Emitting Diodes. *Adv. Funct. Mater.* **2025**, *35*, 2504261.

[S8] Kim, J. M.; Choi, D.; Lee, N.; Chae, W. S.; Kim, H. S.; Yu, J. H.; Lee, J. S. Role of Conjugated Structure of Cross-linkers in Patterned QLEDs. *Nano Lett.* **2025**, *25*, 10435-10441.

[S9] Yang, J.; Lee, M.; Park, S. Y.; Park, M.; Kim, J.; Sitapure, N.; Hahm, D.; Rhee, S.; Lee, D.; Jo, H. et al. Nondestructive Photopatterning of Heavy-Metal-Free Quantum Dots. *Adv. Mater.* **2022**, *34*, 2205504.

[S10] Yang, J.; Hahm, D.; Kim, K.; Rhee, S.; Lee, M.; Kim, S.; Chang, J. H.; Park, H. W.; Lim, J.; Lee, M. et al. High-resolution patterning of colloidal quantum dots via non-destructive, light-driven ligand crosslinking. *Nat. Commun.* **2020**, *11*, 2874.

[S11] Liu, D.; Weng, K.; Zhao, H.; Wang, S.; Qiu, H.; Luo, X.; Lu, S.; Duan, L.; Bai, S.; Zhang, H. et al. Nondestructive Direct Optical Patterning of Perovskite Nanocrystals with Carbene-Based Ligand Cross-Linkers. *ACS Nano* **2024**, *18*, 6896-6907.

[S12] Qie, Y.; Hu, H.; Yu, K.; Zhong, C.; Ju, S.; Liu, Y.; Guo, T.; Li, F. Ligand-Nondestructive Direct Photolithography Assisted by Semiconductor Polymer Cross-Linking for High-Resolution Quantum Dot Light-Emitting Diodes. *Nano Lett.* **2024**, *24*, 1254-1260.

[S13] Lee, N.; Choi, D.; Ko, K. J.; Kim, H. S.; Yu, J. H.; Lee, J. S. Direct Optical Lithography Using Diazirine Cross-Linker for Quantum Dot Light Emitting Diodes and Enhancing Photoluminescence Quantum Yield through Post-treatment. *ACS Nano* **2025**, *19*, 22253-22261.

[S14] Xiao, P.; Ma, J.; Zhang, Z.; Zou, Y.; Luo, H.; Guan, J.; Zhang, J.; Zhou et al. Ligand-engineered direct optical lithography of nanocrystals with industrially compatible solvents. *ACS Nano* **2025**, *19*, 14509-14520.

[S15] Chen, Z.; Man, Z.; Rao, S.; Zhao, J.; Wang, S.; Zhang, R.; Teng, F.; Tang, A. Rigid crosslinker-assisted nondestructive direct photolithograph for patterned QLED displays. *Light Sci. Appl.* **2025**, *14*, 251.

[S16] Guan, J.; Ma, J.; Zhou, L.; Zou, Y.; Ye, L.; Hou, W.; Zhang, P.; Dai, X.; Zhang, H.; Talapin, D. V. et al. Direct ambient photopatterning of RGB quantum dots for light-emitting diodes with EQE exceeding 20%. *Nat. Commun.* **2025**, *16*, 9689.

[S17] Lian, Y.; Wang, Y.; Yuan, Y.; Ren, Z.; Tang, W.; Liu, Z.; Xing, S.; Ji, K.; Yuan, B.; Yang, Y. et al. Downscaling micro- and nano-perovskite LEDs. *Nature* **2025**, *640*, 62-68.

[S18] Jing, Y.; Yao, M.; Yang, M.; Li, M.; Ding, H.; Yang, G.; Zhang, R.; Han, D.; Liu, H.; Zhong, H. Photolithographic fabrication of high-resolution Micro-QLEDs towards color-conversion microdisplay. *Light Sci. Appl.* **2025**, *14*, 370.